Early onset of industrial-era warming across the oceans and continents

Nerilie J. Abram[1,2*], Helen V. McGregor[3], Jessica E. Tierney[4,5], Michael N. Evans[6], Nicholas P. McKay[7], Darrell S. Kaufman[7] and the PAGES 2k Consortium[★]

1. Research School of Earth Sciences, The Australian National University, ACT 2601 Australia.
2. ARC Centre of Excellence for Climate System Science, The Australian National University, ACT 2601 Australia.
3. School of Earth and Environmental Sciences, University of Wollongong, NSW 2522 Australia.
4. University of Arizona, Department of Geosciences, Tucson, AZ 85721 USA.
5. Woods Hole Oceanographic Institution, Woods Hole, MA 02543 USA.
6. Department of Geology and Earth System Science Interdisciplinary Center, University of Maryland, College Park, MD 20742 USA.
7. School of Earth Sciences and Environmental Sustainability, Northern Arizona University, Flagstaff, AZ 86011 USA.
*email: nerilie.abram@anu.edu.au

[★]A list of PAGES (Past Global Changes) 2k Consortium authors that contributed to this work appears at the end of the paper.

The evolution of industrial-era warming across the continents and oceans provides critical context for future climate change, and has fundamental importance for determining climate sensitivity and the processes that control regional warming. Here we use post-1500CE palaeoclimate records to show that sustained, significant warming of the tropical oceans first developed during the mid-19th Century, and was near-synchronous with Northern Hemisphere continental warming. The early onset of industrial-era warming in palaeoclimate records and model simulations suggests greenhouse forcing of industrial-era warming commenced as early as the mid-19th Century, and included an enhanced equatorial ocean response mechanism. The development of Southern Hemisphere warming is delayed in reconstructions, but this apparent delay is not reproduced in climate simulations. Our findings imply that instrumental records are too short to comprehensively assess anthropogenic climate change, and in some regions ~180 years of industrial-era warming has already caused surface temperatures to emerge above pre-industrial variability.

Palaeoclimate data from the past two millennia – a period when natural and anthropogenic climate forcings are reasonably well constrained – provide valuable perspectives on global temperature changes during the 20th Century. Climate reconstructions of the past 2000 years have focused mainly on the Northern Hemisphere (NH)[1-3], using records derived primarily from terrestrial settings. Recent continental-scale temperature reconstructions provided evidence for significant 20th Century warming over all reconstruction regions except Antarctica[4]. A new Southern Hemisphere (SH) temperature reconstruction also demonstrated that the 20th Century is the only period of the last millennium when simultaneous warm extremes occurred across both hemispheres[5]. These valuable hemispheric and regional temperature histories do not, however, allow for assessments of how past temperature changes evolved between the oceans and land.

The oceans represent a significant heat reservoir, taking up more than 90% of the total global energy imbalance since the 1950s[6]. Internal variability of ocean circulation mediates the global climate and is, for example, implicated in the slowdown of global atmospheric warming during the 2001–2014CE "hiatus" interval[7] because of the drawdown of additional heat into the sub-surface ocean[7,8]. The significance of the recent warming slowdown is debated[9]; however, earlier decade-scale plateaus in the rate of warming are prominent features of the climate record[10]. Given the importance of the oceans in determining the pace and regional structure of climate changes[11], it is essential to understand how anthropogenic warming developed in the oceans and over land during the Industrial Era.

Determining an unambiguous time for the start of the Industrial Era is difficult, and forms part of the debate over a formal definition of the Anthropocene[12,13]. The Intergovernmental Panel on Climate Change (IPCC) uses "Industrial Era" to refer, somewhat arbitrarily, to the time after 1750CE when industrial growth began in Britain, spread to other countries, and led to a strong increase in fossil fuel use and greenhouse gas emissions. In this study, the term "industrial-era warming" refers to the sustained, significant warming of Earth's climate that developed during the Industrial Era. We use the palaeoclimate history since 1500CE as context for assessing the evolution of industrial-era warming across surface-ocean and land areas. Our assessments use newly developed regional sea surface temperature (SST) reconstructions for the tropical oceans[14] and SST-sensitive records for the global oceans[14,15], alongside continental-scale temperature reconstructions and databases[4,16] (Fig. 1; Methods). We compare the onset of industrial-era

warming in these palaeoclimate datasets to transient multi-model climate simulations driven by full natural and anthropogenic forcings[17]. We also use experiments with single[18-20] and cumulative[21] external climate forcings to investigate the factors defining the onset of industrial-era warming.

Regional features of industrial-era warming

Synthesis of marine palaeoclimate records spanning the past 2000 years has identified a robust global surface-ocean cooling trend that reached coolest conditions during ~1400–1800CE[15]. This is qualitatively consistent with pre-industrial cooling trends in terrestrial records, and can be explained by an increased frequency of explosive volcanism during the past millennium[15,22]. Marine records with moderate-to-high (<25y) temporal resolution indicate that in many regions this long-term SST cooling trend reversed during the Industrial Era[14,15], including in the tropical oceans where robust regional SST reconstructions spanning the past four centuries have been developed using coral archives[14]. Industrial-era warming in the area-weighted average of regional tropical SST reconstructions is visually similar to warming of the global area-weighted mean of terrestrial temperature reconstructions[4] (Fig. 1c-d). In particular, the average terrestrial and tropical ocean temperature histories show industrial-era warming developing after 1800CE, with similar multi-decadal expressions of accelerated and reduced warming phases.

The similarity of average terrestrial and marine temperature histories (Fig. 1c-d) masks important regional differences in industrial-era warming (Fig. 2; Extended Data Fig. 1). To examine these regional features, we first assess when sustained, significant warming began in the regional temperature reconstructions. We define a sustained and significant trend as the most recent trend that persists until the end of the reconstruction and is significantly different from zero above the 90% confidence level ($p<0.1$). We determine the median time of onset of these sustained trends across different levels of smoothing (15-50y) applied to the regional reconstructions (Methods; Extended Data Fig. 2a)[23,24]. The strengths and limitations of this and other changepoint detection methods in assessing the onset of industrial-era warming are explored using synthetic time series (Methods; Extended Data Fig. 3). Model-based testing suggests that estimates for warming onset are insensitive to the seasonal preference that exists in some regional reconstructions[4] (Methods; Extended Data Fig. 4).

Sustained, significant warming began in the tropical oceans around the 1830s, with no discernible difference in onset across the three tropical SST reconstruction regions (Fig. 2a; Table 1; Extended Data Fig. 1a-b). The onset of tropical-ocean warming is similar to the median onset of warming in NH mean temperature[3] (Extended Data Fig. 1a), although the NH ensemble does also include a sub-member where recent warming is not sustained to the end of the reconstruction (Supplementary Figure 1). This is due to strong multi-decadal variability, which is common to each of the NH mid-latitude continental regions and can delay the detection of sustained warming trends at narrow filter widths (Extended Data Fig. 5). Nevertheless, each of the NH regional-scale reconstructions also display mid-19th Century onsets for industrial-era warming (Fig. 2a; Table 1; Extended Data Fig. 1a-b).

In contrast to the mid-19th Century onset of warming in the tropical oceans and the NH, the SH onset of industrial-era warming appears delayed (Fig. 2a; Table 1). In hemispheric-scale reconstructions[3,5], the median estimate for the onset of sustained warming is ~50 years later in the SH than the NH (Extended Data Fig. 1a; Supplementary Figure 1). The regional structure of this apparent SH lag involves sustained, significant warming developing over Australasia and South America around the start of the 20th Century, while significant continent-scale warming is not detected for Antarctica (Table 1; Extended Data Fig. 1a). We note that the Antarctic reconstruction has the greatest uncertainty of the regional reconstructions[4] (methods), and that significant warming has been documented over the Antarctic Peninsula and West Antarctica since the mid-20th Century[23,25]. However, the absence of significant Antarctic warming at the continent-scale is corroborated by post-1979 satellite observations averaged across Antarctica[26].

Industrial-era warming across the oceans and continents is further investigated by examining the rates of regional warming. All century-scale linear trends in the regional reconstructions since 1500CE are calculated (100y trends with 1y time step; Supplementary Animation 1), and the distributions of trends beginning since 1800CE are used to assess the regional rates of industrial-era warming. For each tropical ocean and NH regional reconstruction the distribution of century-scale trends starting after 1800CE has a clear positive shift compared to earlier trends (Fig. 2b; Table 1; Extended Data Fig. 1c), and includes the largest century-scale warming trend of the past ~500 years. Temperature trends in the Arctic since 1800CE are greater than in any other region, indicative of Arctic amplification[27]. The similarity of post-1800CE trends for

the tropical Indian and western Atlantic oceans with those in Europe, Asia and North America (Table 1), indicates that industrial-era warming of the tropical oceans has progressed at a rate similar to warming of the NH mid-latitude continents. In contrast, rates of century-scale warming since 1800CE in the SH regional reconstructions are slower than for the tropical oceans and NH continents (Fig. 2b; Table 1). This may be related to the delayed onset of warming in the Australasia and South America reconstructions, but it is also consistent with instrumental evidence for hemispheric asymmetries in the rate of 20th Century warming (Fig. 1a-b). For Antarctica, the absence of continent-scale warming during the Industrial Era results in pre- and post-1800CE trend distributions that are statistically indistinguishable (Extended Data Fig. 1c).

The time when a climate change signal exceeds the range of climate variability is known as the Time of Emergence (ToE)[28]. The ToE for industrial-era warming depends upon: (i) when warming began, (ii) the rate of warming, and (iii) the magnitude of interannual to multi-decadal climate variability. ToE studies typically use 20th Century instrumental data or post-1850 (historical) simulations to characterise the baseline climate, and have commonly concluded that unprecedented climates will emerge first in tropical air temperatures because of the small magnitude of variability in these regions[28-30]. However, our findings of a mid-19th Century onset of industrial-era warming suggest that in some regions the entire instrumental period contains a signature of climate warming, rendering it unsuitable for determining climate emergence. We use the multi-century context available from the regional palaeoclimate reconstructions, and a pre-1800CE reference period (Methods), to assess the extent to which industrial-era warming may have already emerged in regional climates.

Industrial-era warming led to regional climate change emergence first in the Arctic (Fig. 2c, Table 1). Despite the large variability of Arctic climate, palaeoclimate ToE assessment indicates that the early onset and rapid rate of warming resulted in climate change emergence during the 1930s (~100 years after sustained, significant warming began). The tropical ocean regions display a similar rate of warming to the NH mid-latitude continents, but the industrial-era warming signal emerges sooner in the tropical oceans (ToE at ~1948–1962CE) because of the smaller magnitude of variability here. Emergence of industrial-era warming for Australasia is around ~1960CE, as the delayed onset of warming is compensated by the small magnitude of interannual variability in this regional reconstruction. All other regions apart from Antarctica are nearing the emergence of warming

above the threshold of pre-industrial climate variability by the start of the 21st Century (i.e. the end of the reconstructions).

Our regional palaeoclimate assessments suggest that widespread climate warming observed during the 20th Century forms part of a sustained trend that began in the tropical oceans and over some NH land areas around the 1830s (~180 years ago). Although caveats exist about how accurately regional palaeoclimate reconstructions represent past temperature changes[4,14-16], our multi-century assessments clearly demonstrate the need to incorporate pre-20th Century information in comprehensive assessments of industrial-era warming. The early onset of industrial-era warming may not alter the conclusions of ToE studies focused on protecting infrastructure built during recent decades[31]. However, our findings imply that ToE studies relying on a 20th-Century baseline may underestimate how soon climate change impacts will fall outside of the range of climate variability to which natural systems are adapted[30].

Climate forcing of industrial-era warming

Model simulations provide an important tool for investigating which forcings are most consistent with the reconstructed onset of industrial-era warming. We examine the regional responses of global climate model simulations to natural and anthropogenic forcings since 1500CE, applying the same trend detection methodology used for the palaeoclimate reconstructions (Methods). An ensemble of ten different models (Extended Data Table 2) reproduces the near-synchronous mid-19th Century onset of sustained, significant warming observed for reconstructed NH surface air temperature and tropical SST (Fig. 3a; Table 1). Palaeoclimate data-model agreement is particularly good for NH terrestrial regions, where the patterns of short-term cooling caused by volcanic eruptions and sustained recent warming from greenhouse gas emissions are remarkably similar (Extended Data Fig. 2). The agreement between the multi-model ensemble and palaeoclimate reconstructions suggests that the onset of industrial-era warming over NH landmasses and in the tropical oceans is consistent with a forced climate response.

In contrast, none of the climate models show evidence for a delayed SH onset of industrial-era warming (Fig. 3a). A 10-member ensemble of LOVECLIM simulations also suggests that the delayed development of warming over Antarctica and Australasia is not explicable within the range of unforced climate variability in that model (Fig. 3b). Instead, the evolution of regional

temperature trends in the multi-model ensemble mean (Extended Data Fig. 2b) and within individual models (Supplementary Figure 2) shows a globally synchronous thermodynamic response of surface temperatures to external climate forcings. Previous palaeoclimate studies have noted that climate models tend to overemphasise NH-SH synchronicity of past temperature changes[5,32], perhaps by overestimating externally forced climate responses in the SH, and/or underestimating the magnitude of SH climate variability[32]. Unresolved or misrepresented physical processes in model representations of the SH ocean-atmosphere-cryosphere systems also hinder the accurate simulation of SH climate[26,33], including the overestimation of simulated Antarctic-region warming compared with satellite observations of recent surface air and ocean temperature trends[26]. The paucity of climate observations also hinders attempts to resolve differences between observations and simulations in the SH[26,32]. As a result, currently available model output cannot be reasonably interrogated to assess the delayed onset of SH industrial-era warming suggested by palaeoclimate observations.

Naturally forced climate cooling may have helped set the stage for the widespread onset of industrial-era warming in the tropical oceans and over NH landmasses during the mid-19th Century. Episodic cooling caused by the large 1815 Tambora volcanic eruption is prominent in NH terrestrial temperature reconstructions (Fig. 2a). In Last Millennium model simulations, the strong cooling caused by the Tambora eruption is followed immediately by a decade-scale interval of accelerated global warming as the climate recovers[34]. The Dalton solar minimum also occurred in the early 19th Century, but solar forcing is thought to have only a small influence on last millennium climate compared to the effects of volcanic eruptions[20]. In the CSIRO Mk3L experiments, where forcings were applied cumulatively rather than individually, it is particularly the addition of volcanic forcing that tends to focus the onset of industrial-era warming to a narrower time window – both between regions and between ensemble members for the same region – compared to experiments run with greenhouse forcing alone (Fig. 3c).

Simulations suggest that recovery from volcanic cooling is not an essential requirement for reproducing the mid-19th Century onset of industrial-era warming. Multi-model experiments forced only with greenhouse gases capture regional onsets for sustained industrial-era warming consistent with the tropical ocean and NH continental reconstructions (Fig. 3d). Testing of our changepoint detection method also indicates that volcanic-style cooling events do not substantially alter the

onset determined for sustained warming trends in synthetic time series (Methods, Extended Data Fig. 3a-b). We conclude that greenhouse forcing of industrial-era warming likely began by the mid-19th Century, but the confluence of explosive volcanic eruptions around this time was probably also influential in aligning the onset of warming over tropical-ocean and NH land regions.

Mechanisms of industrial-era warming

Our regional palaeoclimate assessments show that the thermodynamic response to increasing greenhouse gas concentrations developed in the oceans and atmosphere even when anthropogenic contributions were small. The spatial fingerprint of the onset of industrial-era warming may further elucidate the role of the oceans in the development of anthropogenic warming. We explore this by assessing changepoints in the site-level palaeoclimate records that contribute to the marine[14,15] and terrestrial[4,16] temperature reconstructions (Extended Data Fig. 6). Onset estimates from site-level records are more variable than for the regional reconstructions. This arises from: (i) lower trend-to-variability (or signal-to-noise) ratios in individual palaeoclimate records, (ii) varying lengths of the individual records that do not always include information before the onset of sustained industrial-era trends, and (iii) differences in how representative each record is of local temperature. Similar issues (i–ii) limit climate change detection and attribution at sub-regional scales from climate observations and simulations[35]. For these reasons we view the site-level analyses in a qualitative sense only (Fig. 4), using them to aid the more robust assessments derived from regional reconstructions (Fig. 2).

Sustained and significant warming trends developed during the Industrial Era across the majority (71%, n = 55) of marine records (Extended Data Fig. 6a). This complements similar findings of widespread recent warming trends in site-level palaeoclimate records from predominantly terrestrial environments[4]. Development of sustained warming during the 19th Century in individual records from the tropical oceans and in NH mid- and high-latitude terrestrial records (Fig. 4) corroborate our findings based on the regional reconstructions. Some SH mid-latitude terrestrial records also show this early warming (Fig. 4a), suggesting that while continental-scale temperature reconstructions for Australasia and South America indicate a delayed onset of industrial-era warming (Fig. 2), this may not be representative of all SH mid-latitude land areas (Fig. 4a).

The early onset of industrial-era warming of the tropical oceans was widespread; however, industrial-era climate changes may have resulted in localised surface-ocean cooling in some settings (Extended Data Fig. 6b, 7a). Previous assessments of the moderately resolved marine records cautiously concluded that qualitative warming and cooling trends during the 20th Century were produced if the records were composited into *a priori* defined non-upwelling and upwelling subsets, or if the records were composited by tropical versus NH extratropical location, or by proxy type[15]. Our changepoint assessment of the moderately resolved marine records finds that the most distinct differentiation between recent cooling and warming trends occurs when the records are separated into upwelling and non-upwelling sites (Extended Data Fig. 7b-d). Thus enhanced ocean upwelling may be the most plausible mechanism for explaining the recent cooling trends detected at some marine sites, consistent with theories that climate warming could, in some locations, cause strengthening of the surface winds that generate coastal upwelling[36-38].

The early development and rapid rate of tropical-ocean warming during the Industrial Era (Fig. 2, Fig. 4b) may corroborate model-based descriptions of an enhanced equatorial response (EER) of the oceans to increased greenhouse forcing[39,40]. The EER warming near the equator is caused by increased surface ocean stability and a reduction in surface evaporative cooling due to the combination of lower wind speed and relative humidity. The hypothesised EER mechanism and spatial fingerprint differs from an El Niño-like response of the tropical oceans to global warming (requiring weaker Walker circulation, reduced eastern Pacific upwelling and reduced east-west SST gradient)[41], and shows greater consistency between models[39]. A regional SST reconstruction for the eastern Pacific, although not used in our study because it is thought to have a spuriously large 20th Century trend attributed to hydrologic effects[14], indicates that sustained, significant warming of eastern Pacific SST began markedly later (~1913CE) than in the other tropical ocean regions[14]. Full-forcing and greenhouse-only climate model simulations assessed spatially at 5^{o}x5^{o} grid resolution (Extended Data Fig. 8) also display a delayed onset of industrial-era warming in the eastern Pacific over a narrow region along the equator, distinct from the otherwise widespread early onset of tropical surface-ocean warming (Extended Data Fig. 8, Supplementary Figure 3). The delayed detection of sustained, significant warming in the eastern Pacific may be influenced by large-amplitude interannual variability here (Extended Data Fig. 3b-c), which limits our ability to confidently evaluate El Niño (or La Niña)-like dynamic mechanisms in defining the onset of industrial-era warming across the oceans. Nevertheless, the early onset of industrial-era warming in

tropical ocean regions away from the equatorial eastern Pacific, in reconstructions and simulations, appears to support an enhanced equatorial response in the SST changes caused by global warming.

Widespread warming of tropical SSTs during the Industrial Era (Fig. 2, Fig. 4b) may have had global significance because of the non-linear influence of tropical SSTs on deep atmospheric circulation, which redistributes heat and moisture. The latitudinal development of terrestrial warming that we observe across individual palaeoclimate records (Fig. 4a) is similar to that reported for 20th-Century terrestrial air temperature observations[42]. In that study it was proposed that 20th-Century terrestrial warming focused over the NH subtropical-subpolar regions and in a narrow band over the SH subtropics could be indicative of anthropogenically forced widening of the tropics through expansion of the Hadley circulation cells[42]. The causes of recent multi-decadal episodes of contraction and expansion of Hadley circulation[43,44] have proven difficult to resolve because of the brevity of observational datasets. However, numerous studies suggest that tropical-ocean warming is essential for reproducing the recent poleward expansion of the Hadley Circulation, because of the effect of SST on tropospheric temperature, tropopause height and baroclinic wave position and stability[45,46]. Further assessments of marine and terrestrial palaeoclimate networks, including compilations of hydroclimate-sensitive records currently in development, have the potential to provide valuable context on the role of rapid tropical ocean warming during the Industrial Era in widening the tropical climate belt.

SH reconstruction-simulation differences, and the lack of suitable palaeoclimate records from the extratropical SH oceans, currently preclude an assessment of the role of the oceans in the delayed onset of Antarctic warming seen in regional (Fig. 2) and site-level (Fig. 4a) palaeoclimate analyses, as well as observational records[26]. Idealised model experiments of ocean heating predict a centennial-scale delayed onset of anthropogenic warming in the Southern Ocean caused by upwelling of unmodified subsurface water and northward advection of any surface warming signal[11,47]. Strengthening westerly winds over the Southern Ocean during the 20th Century, related to the Southern Annular Mode[48], have likely also influenced the delayed development of sustained industrial-era warming over Antarctica. In the NH, the scarcity of suitable marine palaeoclimate records from the mid- to high-latitudes also precludes an assessment of ocean-land relationships during the onset of industrial-era warming. We do, however, find that in full-forcing and greenhouse-only simulations the onset of sustained surface-ocean warming in the North Atlantic

Ocean is delayed, or instead characterised by cooling (Extended Data Fig. 8). This is consistent with reports of an unusual slowdown of Atlantic Meridional Overturning circulation during the 20th Century[49]. Increasing knowledge of the temperature evolution of the extratropical oceans before and during the Industrial Era should be considered a major target for future palaeoclimate research.

The spatial development of industrial-era warming across the oceans and continents demonstrates that the tropical oceans and Northern Hemisphere were particularly responsive to the climate forcings that shaped industrial-era warming. The mid-19th Century commencement of industrial-era warming suggests that Earth's surface temperature may respond to even small increases in greenhouse gas forcing more rapidly than previously thought[50], and highlights the importance of multi-century palaeoclimate records and model simulations in assessing the response of worldwide climate to anthropogenic greenhouse gas emissions.

References

1 Hegerl, G. C., Crowley, T. J., Hyde, W. T. & Frame, D. J. Climate sensitivity constrained by temperature reconstructions over the past seven centuries. *Nature* **440**, 1029-1032, doi:10.1038/nature04679 (2006).

2 Mann, M. E. *et al.* Proxy-based reconstructions of hemispheric and global surface temperature variations over the past two millennia. *Proceedings of the National Academy of Sciences* **105**, 13252-13257, doi:10.1073/pnas.0805721105 (2008).

3 Frank, D. C. *et al.* Ensemble reconstruction constraints on the global carbon cycle sensitivity to climate. *Nature* **463**, 527-530, doi:10.1038/nature08769 (2010).

4 PAGES 2k Consortium. Continental-scale temperature variability during the past two millennia. *Nature Geoscience* **6**, 339-346, doi:10.1038/ngeo1797 (2013).

5 Neukom, R. *et al.* Inter-hemispheric temperature variability over the past millennium. *Nature Climate Change* **4**, 362-367, doi:10.1038/nclimate2174 (2014).

6 Levitus, S. *et al.* World ocean heat content and thermosteric sea level change (0–2000 m), 1955–2010. *Geophysical Research Letters* **39**, L10603, doi:10.1029/2012gl051106 (2012).

7 England, M. H. *et al.* Recent intensification of wind-driven circulation in the Pacific and the ongoing warming hiatus. *Nature Clim. Change* **4**, 222-227, doi:10.1038/nclimate2106 (2014).

8 Chen, X. & Tung, K.-K. Varying planetary heat sink led to global-warming slowdown and acceleration. *Science* **345**, 897-903, doi:10.1126/science.1254937 (2014).

9 Karl, T. R. *et al.* Possible artifacts of data biases in the recent global surface warming hiatus. *Science*, doi:10.1126/science.aaa5632 (2015).

10 Crowley, T. J., Obrochta, S. P. & Liu, J. Recent global temperature “plateau” in the context of a new proxy reconstruction. *Earth's Future* **2**, 281-294, doi:10.1002/2013EF000216 (2014).

11 Marshall, J. *et al.* The ocean’s role in the transient response of climate to abrupt greenhouse gas forcing. *Clim Dyn* **44**, 2287-2299, doi:10.1007/s00382-014-2308-0 (2015).

12 Lewis, S. L. & Maslin, M. A. Defining the Anthropocene. *Nature* **519**, 171-180, doi:10.1038/nature14258 (2015).

13 Ruddiman, W. F. The Anthropocene. *Annual Review of Earth and Planetary Sciences* **41**, 45-68, doi:doi:10.1146/annurev-earth-050212-123944 (2013).

14 Tierney, J. E. *et al.* Tropical sea-surface temperatures for the past four centuries reconstructed from coral archives. *Paleoceanography*, doi:10.1002/2014PA002717 (2015).

15 McGregor, H. V. *et al.* Robust global ocean cooling trend for the pre-industrial Common Era. *Nature Geosci* **8**, 671-677, doi:10.1038/ngeo2510 (2015).

16 McKay, N. P. & Kaufman, D. S. An extended Arctic proxy temperature database for the past 2,000 years. *Scientific Data* **1**, doi:10.1038/sdata.2014.26 (2014).

17 Schmidt, G. A. *et al.* Climate forcing reconstructions for use in PMIP simulations of the last millennium (v1.0). *Geoscientific Model Development* **4**, 33-45, doi:10.5194/gmd-4-33-2011 (2011).

18 Crespin, E., Goosse, H., Fichefet, T., Mairesse, A. & Sallaz-Damaz, Y. Arctic climate over the past millennium: Annual and seasonal responses to external forcings. *The Holocene* **23**, 321-329, doi:10.1177/0959683612463095 (2013).

19 Otto-Bliesner, B. L. *et al.* Climate Variability and Change since 850 C.E.: An Ensemble Approach with the Community Earth System Model (CESM). *Bulletin of the American Meteorological Society*, doi:10.1175/BAMS-D-14-00233.1 (2015).

20 Schurer, A. P., Tett, S. F. B. & Hegerl, G. C. Small influence of solar variability on climate over the past millennium. *Nature Geoscience* **7**, 104-108, doi:10.1038/ngeo2040 (2014).

21 Phipps, S. J. *et al.* Paleoclimate data–model comparison and the role of climate forcings over the past 1500 years. *Journal of Climate* **26**, 6915-6936, doi:10.1175/jcli-d-12-00108.1 (2013).

22 Sigl, M. *et al.* Timing and climate forcing of volcanic eruptions for the past 2,500 years. *Nature* **523**, 543-549, doi:10.1038/nature14565 (2015).

23 Abram, N. J. *et al.* Acceleration of snow melt in an Antarctic Peninsula ice core during the twentieth century. *Nature Geosci* **6**, 404-411, doi:10.1038/ngeo1787 (2013).

24 Chaudhuri, P. & Marron, J. S. SiZer for exploration of structure in curves. *Journal of the American Statistical Association* **94**, 807-823 (1999).
25 Steig, E. J. *et al.* Warming of the Antarctic ice-sheet surface since the 1957 International Geophysical Year. *Nature* **457**, 459-462, doi:10.1038/nature07669 (2009).
26 Jones, J. M. *et al.* Assessing recent trends in high-latitude Southern Hemisphere surface climate. *Nature Climate Change* (in press).
27 Screen, J. A. & Simmonds, I. The central role of diminishing sea ice in recent Arctic temperature amplification. *Nature* **464**, 1334-1337, doi:10.1038/nature09051 (2010).
28 Hawkins, E. & Sutton, R. Time of emergence of climate signals. *Geophysical Research Letters* **39**, L01702, doi:10.1029/2011gl050087 (2012).
29 Diffenbaugh, N. & Scherer, M. Observational and model evidence of global emergence of permanent, unprecedented heat in the 20th and 21st centuries. *Climatic Change* **107**, 615-624, doi:10.1007/s10584-011-0112-y (2011).
30 Mora, C. *et al.* The projected timing of climate departure from recent variability. *Nature* **502**, 183-187, doi:10.1038/nature12540 (2013).
31 Lyu, K., Zhang, X., Church, J. A., Slangen, A. B. A. & Hu, J. Time of emergence for regional sea-level change. *Nature Climate Change* **4**, 1006-1010, doi:10.1038/nclimate2397 (2014).
32 PAGES2k-PMIP3 group. Continental-scale temperature variability in PMIP3 simulations and PAGES 2k regional temperature reconstructions over the past millennium. *Clim. Past* **11**, 1673-1699, doi:10.5194/cp-11-1673-2015 (2015).
33 Bracegirdle, T. J., Stephenson, D. B., Turner, J. & Phillips, T. The importance of sea ice area biases in 21st century multimodel projections of Antarctic temperature and precipitation. *Geophysical Research Letters* **42**, 10832-10839, doi:10.1002/2015GL067055 (2015).
34 Schurer, A. P., Hegerl, G. C. & Obrochta, S. P. Determining the likelihood of pauses and surges in global warming. *Geophysical Research Letters* **42**, 5974-5982, doi:10.1002/2015GL064458 (2015).
35 Stott, P. A. *et al.* Detection and attribution of climate change: a regional perspective. *WIRES: Climate Change* **1**, 192-211, doi:10.1002/wcc.34 (2010).
36 Bakun, A. Global climate change and intensification of coastal ocean upwelling. *Science* **247**, 198-201, doi:10.1126/science.247.4939.198 (1990).
37 McGregor, H. V., Dima, M., Fischer, H. W. & Mulitza, S. Rapid 20th-Century increase in coastal upwelling off northwest Africa. *Science* **315**, 637-639, doi:10.1126/science.1134839 (2007).
38 Narayan, N., Paul, A., Mulitza, S. & Schulz, M. Trends in coastal upwelling intensity during the late 20th century. *Ocean Sci.* **6**, 815-823, doi:10.5194/os-6-815-2010 (2010).
39 Liu, Z., Vavrus, S., He, F., Wen, N. & Zhong, Y. Rethinking Tropical Ocean Response to Global Warming: The Enhanced Equatorial Warming. *Journal of Climate* **18**, 4684-4700, doi:10.1175/JCLI3579.1 (2005).
40 Xie, S.-P. *et al.* Global Warming Pattern Formation: Sea Surface Temperature and Rainfall. *Journal of Climate* **23**, 966-986, doi:10.1175/2009JCLI3329.1 (2010).
41 Collins, M. *et al.* The impact of global warming on the tropical Pacific Ocean and El Nino. *Nature Geosci* **3**, 391-397, doi:10.1038/ngeo868 (2010).
42 Ji, F., Wu, Z., Huang, J. & Chassignet, E. P. Evolution of land surface air temperature trend. *Nature Clim. Change* **4**, 462-466, doi:10.1038/nclimate2223 (2014).
43 Bronnimann, S. *et al.* Southward shift of the northern tropical belt from 1945 to 1980. *Nature Geosci* **8**, 969-974, doi:10.1038/ngeo2568 (2015).
44 Seidel, D. J., Fu, Q., Randel, W. J. & Reichler, T. J. Widening of the tropical belt in a changing climate. *Nature Geosci* **1**, 21-24 (2008).
45 Hu, Y., Zhou, C. & Liu, J. Observational evidence for poleward expansion of the Hadley circulation. *Advances in Atmospheric Sciences* **28**, 33-44, doi:10.1007/s00376-010-0032-1 (2011).
46 Staten, P. W., Rutz, J. J., Reichler, T. & Lu, J. Breaking down the tropospheric circulation response by forcing. *Clim Dyn* **39**, 2361-2375, doi:10.1007/s00382-011-1267-y (2012).

47 Armour, K. C., Marshall, J., Scott, J. R., Donohoe, A. & Newsom, E. R. Southern Ocean warming delayed by circumpolar upwelling and equatorward transport. *Nature Geosci*, doi:10.1038/ngeo2731 (2016).
48 Abram, N. J. *et al.* Evolution of the Southern Annular Mode during the past millennium. *Nature Clim. Change* **4**, 564-569, doi:10.1038/nclimate2235 (2014).
49 Rahmstorf, S. *et al.* Exceptional twentieth-century slowdown in Atlantic Ocean overturning circulation. *Nature Clim. Change* **5**, 475-480, doi:10.1038/nclimate2554 (2015).
50 Ricke, K. L. & Caldeira, K. Maximum warming occurs about one decade after a carbon dioxide emission. *Environmental Research Letters* **9**, 124002, doi:10.1088/1748-9326/9/12/124002 (2014).

Supplementary Information is available in the online version of the paper.

Acknowledgements We thank the many scientists who made their published palaeoclimate datasets available via public data repositories. This work developed out of the PAGES (Past Global Changes) Ocean2k working group; we are grateful to Kevin Anchukaitis, Henry Wu, Cyril Giry, Delia Oppo and Vasile Ersek for their contributions to the Ocean2k syntheses, to the more than 75 volunteers who constructed the Ocean2k phase 1 metadatabase[14,15], and to Kevin Anchukaitis and Valerie Trouet for discussions that aided this study. We thank Paola Petrelli, François Klein, and Andrew Schurer for assistance in obtaining model datasets, and Kate McGregor for editorial assistance. We acknowledge support from PAGES funded by the US and Swiss National Science Foundations (NSF) and NOAA, and thank Thorsten Kiefer, Marie-France Loutre and the PAGES 2k steering committee for organisational support. We acknowledge the World Climate Research Programme's Working Group on Coupled Modelling, which is responsible for CMIP, and we thank the climate modelling groups for producing and making available their model output. The U.S. Department of Energy's Program for Climate Model Diagnosis and Intercomparison provides coordinating support for CMIP and led development of software infrastructure in partnership with the Global Organization for Earth System Science Portals.

N.J.A. is supported by an Australian Research Council (ARC) QEII fellowship awarded under DP110101161 and this work contributes to ARC *Discovery Project* DP140102059 (N.J.A, M.A.J.C) and the ARC Centre of Excellence for Climate System Science (N.J.A., S.J.P., J.G.). H.V.M. is supported by ARC Future Fellowship FT140100286 and acknowledges funding from ARC *Discovery Project* DP1092945 (H.M.V., S.J.P.). We acknowledge fellowship support from CSIC-Ramón y Cajal post-doctoral programme RYC-2013-14073 (B.M.), Clare Hall College Cambridge Shackleton Fellowship (B.M.), and ARC DECRA fellowship DE130100668 (J.G.). We acknowledge research support from US NSF grant OCE1536249 (M.N.E.), the ARC Special Research Initiative for the Antarctic Gateway Partnership (Project ID SR140300001; S.J.P.), Red CONSOLIDER GRACCIE CTM2014-59111-REDC (B.M.), Swiss NSF grant PZ00P2_154802 (R.N.), the Danish Council for Independent Research, Natural Science OCEANHEAT project 12-126709/FNU (M.-S.S.), the National Natural Science Foundation of China (41273083; K.S.) and Shanghai Fund (2013SH012; K.S.). This is University of Maryland Center for Environmental Science contribution 5206.

Author Contributions N.J.A. designed the study with input from H.V.M., J.E.T., M.N.E, N.P.M. and D.S.K. The palaeoclimate data and model analysis was led by N.J.A. with assistance provided by R.N., K.T., B.M., H.G., S.J.P. and E.J.S.; R.N. and J.G. produced the terrestrial Australasia2k reconstruction; N.J.A., J.E.T., M.N.E., K.H.K., C.P.S. and J.Z. contributed expertise on the high-resolution marine database and reconstructions; H.V.M., M.N.E., B.M., K.T., G.L., J.A.A., P.G.M., M.-S.S., M.-A.S., K.S. and H.L.F. contributed expertise on the moderate-resolution marine database; H.G., S.J.P. and N.J.A. contributed expertise on climate model output, and N.P.M., D.S.K., R.N., E.J.S., J.G., M.A.J.C. and L.v.G. contributed expertise on the terrestrial databases and reconstructions. All authors contributed to discussions that shaped the study and the manuscript. N.J.A. led the writing with contributions from all authors.

Author Information The data and code needed to reproduce results accompany this paper as Supplementary Information. Reprints and permissions information is available at www.nature.com/reprints. The authors declare no competing financial interests. Correspondence and requests for materials should be addressed to N.J.A. (nerilie.abram@anu.edu.au).

⋆PAGES 2k Consortium authors who contributed to this study are:

Kaustubh Thirumalai[8], Belen Martrat[9,10], Hugues Goosse[11], Steven J. Phipps[12,13,14], Eric J. Steig[15,16], K. Halimeda Kilbourne[5,17], Casey P. Saenger[18], Jens Zinke[19,20,21], Guillaume Leduc[22], Jason A. Addison[23], P. Graham Mortyn[24], Marit-Solveig Seidenkrantz[25], Marie-Alexandrine Sicre[26], Kandasamy Selvaraj[27], Helena L. Filipsson[28], Raphael Neukom[29], Joelle Gergis[30,31], Mark A.J. Curran[32] and Lucien von Gunten[33].

Affiliations:

8. Institute for Geophysics, Jackson School of Geosciences, University of Texas, Austin, Texas 78758, USA.
9. Department of Environmental Chemistry, Institute of Environmental Assessment and Water Research (IDÆA), Spanish Council for Scientific Research (CSIC), 08034 Barcelona, Spain.
10. Department of Earth Sciences, Downing Street, University of Cambridge, Cambridge CB2 3EQ, UK.
11. Earth and Life Institute, Université de Louvain, Place pasteur 3, 1348 Louvain-la-Neuve, Belgium.
12. ARC Centre of Excellence for Climate System Science, University of New South Wales, Sydney NSW 2052, Australia.
13. Climate Change Research Centre, University of New South Wales, Sydney NSW 2052, Australia.

14. Institute for Marine and Antarctic Studies, University of Tasmania, Hobart, TAS 7001, Australia.
15. School of Geosciences, University of Edinburgh, Edinburgh EH9 3FE, U.K.
16. Department of Earth and Space Sciences, University of Washington, Seattle, WA 98195 USA.
17. Chesapeake Biological Laboratory, University of Maryland Center for Environmental Science, Solomons, Maryland 20688, USA.
18. Joint Institute for the Study of the Atmosphere and Ocean, University of Washington, Seattle, Washington, USA.
19. Curtin University of Technology, Department of Environment & Agriculture, Bentley, WA 6845, Australia
20. Australian Institute of Marine Science, 39 Fairway, Nedlands, WA 6009, Australia
21. Institute of Geological Sciences, Section Palaeontology, Freie Universität Berlin, Malteserstrasse 74-100,12249 Berlin, Germany.
22. Aix Marseille Université, CNRS, IRD, CEREGE UM34, 13545 Aix-en-Provence Cedex 4, France.
23. U.S. Geological Survey, 345 Middlefield Rd., MS 910, Menlo Park, CA 94025, USA.
24. Universitat Autonoma de Barcelona, Institute of Environmental Science and Technology (ICTA) and Department of Geography, Bellaterra 08193, Spain.
25. Centre for Past Climate Studies and Arctic Research Centre, Department of Geoscience, Aarhus University, Hoegh-Guldbergs Gade 2, DK-8000 Aarhus C, Denmark.
26. Sorbonne Universités (UPMC, Univ Paris 06)-CNRS-IRD-MNHN, LOCEAN Laboratory, 4 place Jussieu, F-75005 Paris, France.
27. State Key Laboratory of Marine Environmental Science and Department of Geological Oceanography, Xiamen University, Xiamen-361102, China.
28. Department of Geology, Lund University, Sölvegatan 12, SE-223 62 Lund, Sweden.
29. Oeschger Centre for Climate Change Research and Institute of Geography, University of Bern, 3012 Bern, Switzerland.
30. School of Earth Sciences, University of Melbourne, Victoria 3010, Australia.
31. ARC Centre of Excellence for Climate System Science, University of Melbourne, Victoria 3010, Australia.
32. Australian Antarctic Division and Antarctic Climate and Ecosystems Cooperative Research Centre, Hobart, Tasmania 7000, Australia.
33. PAGES International Project Office, Falkenplatz 16, 3012 Bern, Switzerland.

Tables

Table 1. Onset, rate and emergence of industrial-era warming in reconstructions and simulations. Statistics represent changes in surface air temperature (SAT) for continental reconstruction regions, and sea surface temperature (SST) for tropical ocean regions. Visual representations of the data in this table are found in Fig. 2a (onset of warming in reconstructions), Fig. 3a (onset of warming in simulations), Fig. 2b (rates of warming) and Fig. 2c (climate emergence).

		Onset of sustained significant warming trends (year CE)		**Century-scale trend distribution (^{o}C 100y^{-1})**		**Emergence (year CE)**
		Recons. Median; 15-50y filter widths	**Simulations** Inter-model median [*25-75% range*]	**Recons. 1500 to 1799CE** median [*25-75% range*]	**Recons. since 1800CE** median [*25-75% range*]	**Recons.** Median; 15-50y filter widths
SAT	Arctic	1831	1843 [*1819 – 1880*]	-0.11 [*-0.41 – 0.07*]	1.07 [*0.92 – 1.26*]	1930
	Europe	1852	1888 [*1840 – 1987*]	0.02 [*-0.39 – 0.33*]	0.46 [*0.29 – 0.58*]	xx (1994)
	Asia	1849	1833 [*1807 – 1999*]	0.00 [*-0.18 – 0.10*]	0.48 [*0.35 – 0.54*]	xx (1987)
	N. America	1847	1859 [*1823 – 1900*]	0.01 [*-0.38 – 0.15*]	0.48 [*0.29 – 0.52*]	xx
SST	W. Atlantic	1828	1836 [*1811 – 1879*]	-0.11 [*-0.21 – 0.01*]	0.41 [*0.27 – 0.51*]	1948
	W. Pacific	1834	1830 [*1818 – 1836*]	-0.09 [*-0.13 – 0.02*]	0.27 [*0.19 – 0.35*]	1962
	Indian	1827	1830 [*1814 – 1838*]	-0.14 [*-0.31 – -0.04*]	0.51 [*0.39 – 0.54*]	1962
SAT	Australasia	1904*	1832 [*1808 – 1833*]	0.00 [*-0.04 – 0.05*]	0.07 [*0.02 – 0.23*]	1959
	S. America	1896	1840 [*1802 – 1880*]	-0.02 [*-0.11 – 0.21*]	0.20 [*-0.02 – 0.38*]	xx
	Antarctica	x	1839 [*1819 – 1851*]	-0.05 [*-0.15 – 0.09*]	-0.06 [*-0.14 – 0.07*]	xx

*c.f. median warming onset of 1886CE in original Australasia2k reconstruction[4] that includes marine SST-sensitive records

x = sustained significant warming never achieved in reconstruction

xx = emergence of industrial-era warming above 1622–1799CE (reference interval) variability not achieved in reconstruction. Years in parentheses refer to emergence within 20 years of the end of the reconstruction making permanent emergence uncertain

Figure legends

Figure 1. Terrestrial and marine palaeoclimate reconstructions. a-b, Instrumental temperature trends from 1961–2010CE for (a) surface air temperature (SAT) and (b) sea surface temperature (SST). Also shown (a) PAGES2k continental-scale reconstruction regions (black boxes)[4], (b) PAGES Ocean2k high-resolution (annual) reconstruction regions (black boxes)[14], and location of highly resolved (blue circles; Extended Data Table 1)[14] and moderately resolved (<25y, purple squares; crossed-squares indicate ocean upwelling sites; Extended Data Fig. 7)[15] marine palaeo-SST proxy records. c-d, 25-year moving averages of, (c) area-weighted mean terrestrial temperature anomaly (brown line)[4,16] and 25–75% range across continental-scale reconstructions (shading), and (d) area-weighted mean tropical SST anomaly (blue line) and range across the Indian, western Pacific and western Atlantic reconstructions[14] (shading). Anomalies relative to 1961–1990CE mean (dashed line).

Figure 2. Onset and magnitude of industrial-era warming in regional temperature reconstructions. a, Regional reconstructions[4,14] since 1500CE (colours) with 15y (thin black) and 50y (thick black) Gaussian smoothing, shown alongside median time of onset for sustained, significant industrial-era warming assessed across 15–50y filter widths (black vertical bars; (Methods; Extended Data Fig. 2a). b, Histograms of century-scale regional trends, comparing trends beginning 1500–1799CE (grey) with trends beginning since 1800CE (colours; y-scaling of regional histograms relative to maximum occurrence to aid visual representation). See Supplementary Animation 1 for temporal evolution of century-scale trends. c, Regional reconstructions with 15y and 50y filters (as in (a)), shown alongside the ±2σ range of interannual variability over 1622–1799CE reference period (shading; +2σ level continued by dashed lines). Median time of climate emergence (black vertical bars) assessed as where the climate signal (15-50y width filters of the regional reconstructions) exceeds the +2σ threshold of the reference period (Methods).

Figure 3. Data-model comparison of industrial-era warming onset. a-d, Median onset of sustained, significant warming in regional reconstructions (grey vertical bars; as in Fig. 2a), shown against, (a) grand-median (blue vertical bar), 25–75% range (box) and 5–95% range (horizontal line) of corresponding regional median warming onsets across 10 multi-model Last Millennium climate simulations with full radiative forcings (Supplementary Fig. 1), (b) median timing (open symbols) of warming onset across 3-member ensembles for single radiative forcing experiments and a 10-member ensemble with full radiative forcings using the LOVECLIM model[18], (c) median timing (open symbols) of warming onset for 3-member ensembles of CSIRO Mk3L simulations using cumulative radiative forcing experiments[21], and (d) grand-median (green vertical bar), 25–75% range (box) and 5–95% range (horizontal line) of regional median warming onsets for 13 ensemble members across four different climate models forced only with greenhouse gas changes[18-21]. Lower panels show corresponding (a) full radiative forcing (blue; from orbital, greenhouse gas, solar and volcanic sources)[17], and (d) equivalent atmospheric CO_2 concentration (green) relative to the mean (dashed line) and ±1.5 interquartile range (grey shading; outlier test) of a 0–1500CE baseline interval. See Extended Data Table 2 for model details.

Figure 4. Latitudinal development of site-level temperature trends. a-b, Cumulative distributions for (a) terrestrial and (b) marine records, showing latitudinal development of sustained significant warming (red; upward) or cooling (blue; downward) trends across the site-level records (Extended Data Fig. 6), expressed as a proportion of total records within each latitudinal band (n-values indicated; grey values denote insufficient site-level records (n≤2) for meaningful

comparison). Light shading (b) denotes significant trends at marine sediment core sites with an *a priori* upwelling regime (Extended Data Fig. 7), where the localised SST response[36-38] to regional climate warming may not be representative of latitudinal average climate. Dashed lines (a-b) show temporal coverage of site-level records (expressed as proportion of latitudinal band total), and (c) the number and type of proxy records available by latitudinal band. Because of the varying length of individual records, not all of which cover the full interval of industrial-era warming (particularly tropical corals), we use these data only as a qualitative indicator of the relative timing of the onset of industrial-era warming between different latitudinal bands.

Methods

Palaeoclimate data. We use the newly developed SST reconstructions and palaeoclimate databases of the PAGES Ocean2k working group. For full details of the data selection criteria and in-depth discussions of the marine datasets and reconstructions see refs. 14 and 15.

The high-resolution (annual or better) component of the Ocean2k dataset consists of 57 coral records (including multiple sensors for some records; Extended Data Table 1) which were used to reconstruct regional mean SST histories for different sectors of the tropical oceans[14]. The SST reconstructions for the tropical Indian, western Pacific and western Atlantic regions are statistically robust over most of the last 400 years[14]. The same reconstruction method applied to the tropical eastern Pacific region yielded poorer statistics and a 20th Century SST trend that is stronger than suggested by instrumental records. This was attributed to non-linear hydrologic effects in the eastern tropical Pacific[14], and hence we exclude this regional reconstruction from the current study. We use the "best" reconstruction for each region, as identified in ref. 14 based on validation statistics from the ensemble of reconstructions produced. From the Ocean2k low-resolution database[15] we use a subset of 21 marine records that are suitable for the recent temperature trend analysis carried out in this study (Extended Data Fig. 7a). These 21 records meet additional criteria of having strong chronological control through ^{210}Pb profiling or counting of annual sediment layers or coral growth bands, as well as an average sample resolution of 25 years or better; we refer to these as moderate-resolution records. The sense of the proxy-temperature response of the high and moderate-resolution ocean palaeoclimate records is based on known physical relationships for the incorporation of geochemical and biological tracers into these records, or based on individually assessed and published temperature-growth relationships.

We compare the ocean records to the continental-scale temperature reconstructions and palaeoclimate databases developed in phase 1 of the PAGES2k project[4], including the updated Arctic v1.1.1 reconstruction and database[16]. For the North America region we use the tree ring-based reconstruction, which has decadal resolution, rather than the lower resolution pollen-derived temperature reconstruction. To avoid record duplication all marine records were removed from the PAGES2k continental database prior to site-level trend analysis. We also exclude the four instrumental records in the South American 2k database from our site-level data assessment so that all information is derived solely from palaeoclimate archives. At the level of regional temperature reconstructions, a small degree of overlap does exist in the contributing data used for

some of the previously published reconstructions. Specifically, nine of the 28 records used for the Australasia2k temperature reconstruction are also used for the tropical western Pacific SST reconstruction, and one is used for the tropical Indian Ocean SST reconstruction. To avoid any bias introduced by data overlap we use a terrestrial-only Australasia2k reconstruction that was produced using the same methodology as the original reconstruction[4] but excludes any of the marine geochemistry records that are used in the Ocean2k high-resolution reconstructions. Details of this terrestrial-only reconstruction, and the reconstruction data and statistics, accompany this paper as Supplementary Data 1. The terrestrial-only reconstruction demonstrates close agreement with the original Australasia2k reconstruction and none of the interpretations in this paper are altered by using the original reconstruction instead of the terrestrial-only version.

Matlab data structures containing the site-level proxy data and regional reconstructions used in this study are provided as Supplementary Data 2, and are archived with the World Data Center for Paleoclimatology at www.ncdc.noaa.gov/paleo/study/20083.

Palaeoclimate data analysis and uncertainties. The analyses performed in this study use annually resolved, unsmoothed input data. For the moderately resolved marine records (resolution given in Extended Data Fig. 7a) and the North America reconstruction (decadal resolution), pseudo-annual data was produced by performing a nearest-neighbour interpolation to produce stepped datasets that continued values across the entire sampling interval that they represent. Chronological uncertainty in the palaeoclimate records and reconstructions is extremely low for the Industrial Era. Annual layer chronologies would be expected to be known to within ±2-3 years back to 1800CE, using conservative estimates and not taking into account the 1815 Tambora eruption that left an unambiguous fixed-time marker in many palaeoclimate archives. Thus, chronological uncertainty in the Industrial Era is well within the level of interpretability of our estimates for the onset of sustained and significant warming based on the changepoint detection method (see *Changepoint method testing*).

The area weightings used to calculate the average tropical ocean temperature histories in Fig. 1d were based on the surface area of the target reconstruction regions on an Earth ellipsoid. These areas are as follows: Indian Ocean = 25.5 x 10^6 km^2, western Pacific = 26.9 x 10^6 km^2, and western Atlantic = 5.1 x 10^6 km^2. The areas of the terrestrial reconstruction regions[4] (Fig. 1c) are:

Arctic = 34.3 x 10^6 km^2, Europe = 13.0 x 10^6 km^2, Asia = 31.1 x 10^6 km^2, North America = 12.5 x 10^6 km^2, Australasia = 37.9 x 10^6 km^2, South America = 20.0 x 10^6 km^2, and Antarctica = 34.4 x 10^6 km^2.

The seasonality of the temperature signal captured by the reconstructions differs between regions. This is due to the availability of site-level palaeoclimate records in each region, some of which only capture climate information related to a specific season (e.g. a summer growing season for trees). Detailed discussion on seasonality can be found in refs. 4,14 and 15. To summarise the information in those primary references: the tropical ocean reconstructions represent April-March (tropical year) annual averages; the Arctic, North America and Antarctic reconstructions represent annual averages; the Australasia reconstruction represents a September-February half-year (warm season) average, and the Europe, Asia and South America reconstructions represent local summer averages. We do not expect the seasonal differences between the regional reconstructions to affect our interpretations of the onset of sustained significant warming between different regions. Changepoint analysis of climate model simulations produces near-identical regional warming onsets when data are compiled as annual averages across all regions or as season-specific averages that match the reported seasonality for each corresponding palaeoclimate reconstruction (Extended Data Fig. 4).

The effect that uncertainty in the regional temperature reconstructions may have on estimates of industrial-era warming onset was assessed using reconstruction ensembles (Extended Data Fig. 1a). Reconstruction ensembles are available for South America, Australasia and the three tropical ocean regions, and were calculated as part of the original reconstruction process by using different methodological choices based on the proxy network, the temperature calibration interval and/or target dataset. We also extend this analysis to reconstruction ensembles available for NH[3] and SH[5] average temperature as an additional test of the apparent SH delay in the onset of industrial-era warming (Extended Data Fig. 1a, Supplementary Figure 1). Uncertainty in the onset of industrial-era warming related to reconstruction uncertainty has a 5%–95% range of within -3y to +25y for the three tropical ocean regions (which each have an average ±2 standard deviation range across reconstruction members of ~0.1^{o}C during the 19th and 20th Centuries). The Australasia ensembles have an average ±2 standard deviation range of 0.4^{o}C during the 19th and 20th Centuries, and there is a -35y to +46y range (5%–95%) in onset estimates determined across this ensemble. The South America ensembles have an average ±2 standard deviation range of 0.6^{o}C during the 19th

and 20th Centuries, and a -16y to +31y range (5%–95%) in the onset of industrial-era warming (Extended Data Fig. 1a).

As a first order estimate, the ranges of onset timings obtained from regions where reconstruction ensembles are available may provide guidance on how reconstruction uncertainty affects other regions. The regional reconstructions for the Arctic and Europe have a similar magnitude of uncertainty during the 19th and 20th Centuries as the South America reconstruction (average ±2 standard deviation of ~0.6°C). Thus uncertainty in the onset of industrial-era warming related to regional reconstruction quality may be similar between these regions. Reconstruction uncertainty is higher for Asia (~0.9°C for ±2RSME) and Antarctica (~1.2°C for ±2 standard error), and so we may expect a larger uncertainty range in onset estimates related to reconstruction quality for these regions. Reconstruction uncertainty for North America is based on decadal resolution data, and so is not directly comparable to the annual resolution of the other regional reconstructions.

Model output. We compare the regional palaeoclimate reconstructions to a multi-model ensemble of transient last millennium simulations from 850CE to 1850CE[51] (Extended Data Table 2), completed as part of the 5th Coupled Model Intercomparison Project (CMIP5). Historical simulations from the same ensemble were used to extend the model output from 1850CE to 2005CE. The CMIP5 last millennium and historical experiments use transient radiative forcings that include orbital, solar, volcanic, greenhouse and ozone parameters, as well as land use changes[17,52]. All data were accessed from the Earth System Grid Federation, with the exception of the historical portions of the HadCM3 simulation (provided by Andrew Schurer, Edinburgh University, UK) and the FGoals-s2 simulation (provided by Tianjun Zhou and Wemin Man, Chinese Academy of Sciences).

Multiple simulations of the last millennium run with LOVECLIM[18] were used to examine climate responses to single radiative forcing scenarios (three ensemble members each), and to assess intra-model variability in full forcing simulations (ten ensemble members). We also examine multiple last millennium simulations of the CSIRO Mk3L coupled climate model run with progressive addition of radiative forcings (three ensemble members each)[21]. The climate response to greenhouse gas forcing alone was further assessed using single forcing experiments of the HadCM3 (four ensemble members)[20] and NCAR CESM1 (three ensemble members)[19] models.

For each of the models we examine surface air temperature (tas field) averaged over the PAGES2k continental palaeoclimate reconstruction regions, and sea surface temperature (tos field) averaged across the PAGES Ocean2k tropical ocean reconstruction regions. Monthly resolution model output was used to generate annual or season-specific averages that correspond to each palaeoclimate reconstruction target region. Because we use the simulations to examine changepoints rather than the magnitude of trends, we do not apply any drift corrections to the model output. Changepoint analysis was performed on individual model runs and then compiled (Fig. 3; Supplementary Figure 2; Extended Data Fig. 8), rather than on ensemble averages to avoid loss of internal variability in the model data.

Matlab data structures containing the model output (compiled as regional time series with annual-average and season-specific resolution) used in this study are provided as Supplementary Data 2, and archived with the World Data Center for Paleoclimatology at www.ncdc.noaa.gov/paleo/study/20083.

Changepoint analysis method. We analyse the trends in the PAGES2k continental and tropical ocean temperature reconstructions (Fig. 2a, Extended Data Fig. 1a), in the site-level terrestrial and marine palaeoclimate databases (Fig. 4, Extended Data Figs. 6 and 7), and in model simulations (Fig. 3, Extended Data Figs. 2 and 8, Supplementary Figures 2 and 3) using the SiZer method[24]. SiZer (SIgnificant ZERo crossings of derivatives) determines the sign and significance of trends in time series data across different levels of smoothing using a Gaussian kernel filter. Following the method used in refs. 23 and 14, we assess climate changepoints from SiZer output by determining the median year of initiation for the most recent significant ($p<0.1$) and sustained trends across smoothing bandwidths spanning all integer years in the range from 15 to 50 years. This range of smoothing levels is designed to reduce the influence of interannual to decadal climate variability on the detection of a sustained trend, while avoiding shifting the true changepoint time if the smoothing window is too long. We assess trends in the time series since 1500CE, and the onset of the most recent significant trend is classified only if the sign of the trend persists through to the most recent end of the record (i.e. a sustained trend). Extended Data Fig. 2a shows the SiZer data used to assess the median initiation point for recent significant warming trends across the continents and tropical oceans in palaeoclimate reconstructions (Fig. 2a). Supplementary Figure 1 shows the SiZer data for multi-model palaeoclimate simulations (Fig. 3a).

Changepoint method testing. Changepoints determined by the SiZer method were tested on a set of synthetic time series with known warming onset (Extended Data Fig. 3). We also compare SiZer estimates for the synthetic warming onset with changepoints determined by linear changepoint methods[53,54]. The synthetic time series were designed to test the performance of changepoint detection methods to different forms of long-term trends, to the presence of volcanic-style cooling events, and to varying magnitudes and redness of variability superimposed upon the trend. Each test was carried out across 1000-member ensembles to generate a distribution of changepoint estimates for each method.

Linear changepoint detection methods best capture the changepoint in synthetic time series when the long-term trend is derived from two straight lines (Extended Data Fig. 3a; series i-ii). However, the SiZer method is more adaptable than linear changepoint methods in detecting the true changepoint in time series where the long-term trend is a curve rather than a straight line (Extended Data Fig. 3a; series iii). This is expected to be advantageous for detecting the initial thermodynamic response to increases in atmospheric greenhouse gas levels, which have an accelerating trajectory during the Industrial Era (Fig. 3d). Previous research has concluded that despite the complexity of the climate system there is a near-linear relationship between global radiative forcing changes and the climate response[10,55]. Hence, we would expect Industrial Era climate trends to be better approximated by a curve rather than a simple straight line.

The addition of synthetic volcanic cooling-style events at the time of, and prior to, the changepoint in synthetic series causes only small deviations in SiZer estimates of the climate changepoint away from the true synthetic changepoint (Extended Data Fig. 3a; series iv-vi). In our tests with a curved (accelerating) warming trend and volcanic-style cooling events centred at 0, -25 and -50 years relative to the onset of the warming trend, the SiZer method returns median times for the warming onset at -1, -9 and -13 years, respectively. This gives us confidence that large volcanic eruptions during the early 19th Century are not likely to have substantially skewed detection of the onset of industrial-era warming trends assessed using the SiZer method.

Finally, we test the sensitivity of changepoint detection methods to the addition of varying climate variability (AR(1) noise) superimposed upon the same long-term warming trend. As the magnitude of climate variability increases, the detection of changepoints becomes progressively later using the SiZer method (Extended Data Fig. 3b). As a result, climate time series from regions

with large interannual to multi-decadal variability may have delayed detection of the onset of industrial-era warming relative to regions with small variability, unless the magnitude of the underlying warming trend is also larger in these regions. In our testing, different levels of lag-1 autocorrelation for the AR(1) noise added to an underlying trend does not alter the median estimate for the onset of warming; however the range of onset estimates about this median becomes greater as autocorrelation increases (Extended Data Fig. 3c).

Across all of the tests examined here the linear intersection and Bayesian changepoint detection methods produce much wider ranges of warming onset estimates than those produced using the SiZer method on the same synthetic ensembles (Extended Data Fig. 3a-c). The linear methods are also less able to detect changepoints for trends that aren't simple linear functions. Based on our changepoint method testing we use the SiZer method in this study as it appears to be most adaptable and stable for dealing with the climate changes that characterise industrial-era warming.

We apply our method testing to assess the range of uncertainty in estimates of the onset of regional warming related to the SiZer changepoint detection method (Extended Data Fig. 1b). This is carried out using an accelerating warming trend upon which AR(1) noise is added that has the same lag-1 autocorrelation and trend:variability characteristics as the regional reconstructions. These parameters are estimated by calculating characteristics of residuals about the 15y filters (as in Fig. 2a) of the regional reconstructions. Uncertainty in onset estimates related to the SiZer method is small, and typically better than ±25 years (5%-95% range). Exceptions are Antarctica, where the small trend relative to variability does not allow for the detection of significant trends, and Asia where strong lag-1 autocorrelation leads to uncertainty in the lower (5%) bound for the onset of warming (Extended Data Fig. 1b).

Emergence testing. We use the regional temperature reconstructions to determine the extent to which industrial-era warming has caused regional climates to emerge above the level of pre-industrial variability. We chose the interval from 1622–1799CE as the climate baseline to test emergence against. The starting point (1622CE) represents the earliest year where temperature reconstructions are available for all of the terrestrial and marine regions examined in this study. The end year (1799CE) was chosen as a time well before the onset of industrial-era warming in any of the regional reconstructions (Table 1). It is also prior to strong volcanic cooling events associated

with the 1809 Unknown and 1815 Tambora eruptions, which could skew the reference period towards cooler states.

Time of Emergence (ToE) is detected when a climate change signal emerges above a defined noise threshold[28]. In this study we use a threshold of 2 standard deviations of interannual variability above the mean of the reference interval (Fig. 2c). We smooth the reconstructions using filters between 15–50y widths (i.e. the same as for our changepoint assessments), and calculate the median time when the climate signal (smoothed reconstructions) emerges and stays above the noise threshold. The emergence year is quite insensitive to the level of smoothing we apply to the climate signal across the 15–50y filter widths used here, with the 5-95% range of emergence estimates being between only 1 and 8 years for the regional reconstructions where climate emergence is found to occur.

A difference in our climate emergence assessment over previously published ToE studies is that the palaeoclimate reconstructions allow us to assess climate emergence using a long baseline interval that occurs entirely prior to the onset of industrial-era warming. Our results demonstrate that in some regions industrial-era warming has already caused climate to emerge above the range of natural variability in the 1622–1799CE reference interval (Table 1). We test the sensitivity of this result to the choice of reference interval and find that all tested reference intervals prior to the onset of industrial-era warming result in similar regional emergence patterns and timings, while reference periods that include parts of the industrial-era warming signal result in later ToE estimates. For example, in the Arctic reconstruction ToE estimates based on different reference periods are: 1947CE (1500–1799CE reference), 1930CE (1600–1799CE reference), 1930CE (1622–1799CE reference; Table 1), 1938CE (1700–1799CE reference), 1960CE (1800–1899CE reference), and 1978CE (1850–1899CE reference). We note that the overlapping interval of the regional reconstructions that we use for our ToE reference (1622–1799CE) occurs during the time of coolest conditions during the past 2000 years[4,15]. Using longer palaeoclimate reference intervals that incorporate earlier, warm intervals of the past 2000 years will alter ToE results, but it is not currently possible to perform this assessment consistently between regions due to the length limitations of currently available tropical ocean temperature reconstructions.

Instrumental data. We plot temperature trends from gridded instrumental datasets in Fig. 1. The sources for these datasets are; surface air temperature from Climate Research Unit (CRU) TS3.22

product[56], the ERAI-f product[57] for surface air temperature over Antarctica, and the HadiSST product[58] for sea surface temperature. The CO_2 equivalent record shown in Fig. 3d is derived from ref. 59.

Code availability. Matlab code for assessing the onset (and sign) of industrial-era climate trends using the SiZer method is archived as Supplementary Data 3 accompanying this manuscript, and with the World Data Center for Paleoclimatology at www.ncdc.noaa.gov/paleo/study/20083. These files include the original SiZer package[24] obtained from http://www.unc.edu/~marron/marron_software.html, as well as additional code to assess the onset of sustained, significant temperature trends in annually resolved climate records.

Methods References

51 Taylor, K. E., Stouffer, R. J. & Meehl, G. A. An overview of CMIP5 and the experiment design. *Bulletin of the American Meteorological Society* **93**, 485-498, doi:10.1175/bams-d-11-00094.1 (2012).

52 Schmidt, G. A. *et al.* Climate forcing reconstructions for use in PMIP simulations of the Last Millennium (v1.1). *Geoscientific Model Development* **5**, 185-191, doi:10.5194/gmd-5-185-2012 (2012).

53 Mudelsee, M. Break function regression. *Eur. Phys. J. Spec. Top.* **174**, 49-63, doi:10.1140/epjst/e2009-01089-3 (2009).

54 Ruggieri, E. A Bayesian approach to detecting change points in climatic records. *International Journal of Climatology* **33**, 520-528, doi:10.1002/joc.3447 (2013).

55 Crowley, T. J. Causes of climate change over the past 1000 years. *Science* **289**, 270-277, doi:10.1126/science.289.5477.270 (2000).

56 Harris, I., Jones, P. D., Osborn, T. J. & Lister, D. H. Updated high-resolution grids of monthly climatic observations – the CRU TS3.10 Dataset. *International Journal of Climatology* **34**, 623-642, doi:10.1002/joc.3711 (2014).

57 Nicolas, J. P. & Bromwich, D. H. New reconstruction of Antarctic near-surface temperatures: multidecadal trends and reliability of global reanalyses. *Journal of Climate* **27**, 8070-8093, doi:10.1175/JCLI-D-13-00733.1 (2014).

58 Rayner, N. A. *et al.* Global analyses of sea surface temperature, sea ice, and night marine air temperature since the late nineteenth century. *Journal of Geophysical Research: Atmospheres* **108**, 4407, doi:10.1029/2002jd002670 (2003).

59 MacFarling Meure, C. *et al.* Law Dome CO_2, CH_4 and N_2O ice core records extended to 2000 years BP. *Geophysical Research Letters* **33**, L14810, doi:10.1029/2006gl026152 (2006).

Extended Data legends

Extended Data Figure 1. Regional distributions of onset estimates for industrial-era warming and post-1800CE warming trends. a, Median (black vertical bars; as in Fig. 2a) onset of sustained, significant warming in regional reconstructions, shown with uncertainty ranges in onset estimates based on available reconstruction ensembles (colours; Methods). Distributions of onset estimates related to reconstruction uncertainty denote median (vertical bars), 25–75% range (boxes) and 5–95% range (horizontal lines). Distributions for the onset of warming are also calculated for NH and SH reconstruction ensembles[3,5], with additional details in Supplementary Figure 1. b, As in a, but for uncertainty ranges in onset estimates based on the SiZer changepoint detection method. Distributions (grey) denote the uncertainty in detecting a known warming onset based on synthetic tests, where 1000 noise series with lag-1 autocorrelation and trend:variability characteristics matching the regional reconstructions are applied to an underlying trend (methods; Extended Data Fig. 3). 'x' symbols are used where low trend:variability characteristics (Antarctica) or high autocorrelation (Asia) limit the detection of a sustained, significant warming trend in the synthetic tests. c, Distribution of century-scale (100y) linear warming trends since 1800CE (coloured bars), shown with reference to the 5–95% range of century-scale trends beginning 1500–1799CE (grey shading). Values denote the percentage of century-scale trends since 1800CE that lie below the 5% level (left) or above the 95% level (right) of trends beginning 1500–1799CE.

Extended Data Figure 2. SiZer trend maps used to assess the onset of sustained significant warming. a, SiZer trend maps[23,24] for each of the regional land and ocean temperature reconstructions. The timing of warming (red) and cooling (blue) trends are calculated at different levels of smoothing. Significant ($p<0.1$) trends are shown by dark red and dark blue shading. Vertical lines indicate the median onset time for the most recent phase of sustained significant warming calculated across 15–50y filter widths (as used in Fig. 2a; Table 1). b, as in (a) but for the ensemble mean of regional surface-air and surface-ocean temperatures across CMIP5 last millennium and historical model simulations. Note that the SiZer analysis for the multi-model ensemble mean is shown for illustrative purposes only and removes the influence of unforced variability to highlight the multi-model thermodynamic response to climate forcings since 1500CE. The multi-model changepoint distributions shown in Fig. 3a are based on SiZer analysis of individual experiments (Supplementary Figure 2), not the ensemble mean shown here. c-d, Radiative climate forcings from greenhouse (green), solar (orange), and volcanic (red) sources since 1500CE[17,52]. For illustrative purposes, the magnitude of short-term forcing from large volcanic events[17,22] exceeds the lower limit of the plot axis.

Extended Data Figure 3. Assessment of changepoint detection methods using synthetic time series. a, Example synthetic time series (grey) consisting of long-term trends with a changepoint at year 0 (black) and AR(1) noise with a lag-1 autocorrelation of 0.1 and ratio of 100y trend:2σ noise of 1:0.5. From top to bottom the synthetic trends represent (i) no trend then linear upward trend, (ii) small linear downward trend then linear upward trend, (iii) small linear downward trend then accelerating upward trend (1/4 sine curve), (iv-vi) as in (iii) but with 10-year long downward excursions centred at (iv) 0 years, (v) -25 years, and (vi) -50 years relative to the onset of the accelerating upward trend. Synthetic trends are designed to capture known features of Earth's climate evolution, namely a long-term gradual pre-industrial cooling trend followed by accelerating industrial-era warming with superimposed episodic volcanic cooling events. Shown for each experiment are the distributions of changepoint results using the SiZer method (blue; this study; Methods), the best-fit intersection of two straight lines[53] (orange) and a Bayesian linear changepoint

method[54] (purple; screening for 1 changepoint and selecting time of maximum probability). Distributions show the median (thick vertical bar), 25–75% range (box) and 5–95% range (thin horizontal line) of changepoints returned across 1000-member ensembles for each test. b, as in (a), but testing the influence of different magnitudes of AR(1) noise on detecting the onset of warming in an underlying trend (using the small linear downward trend then accelerating upward trend, as in test iii). Tests use a ratio of the 100y trend:2σ noise of (vii) 1:0.2, (viii) 1:0.5, (ix) 1:1, and (x) 1:1.5. c, as in (b), but testing the influence of different AR(1) autocorrelation on detecting the onset of warming in an underlying trend. Tests use lag-1 autocorrelations of (xi) 0.1, (xii) 0.3, (xiii) 0.5 and (xiv) 0.7. See Methods for a detailed discussion of these changepoint method tests, and Extended Data Fig. 1b for application of the SiZer method tests using signal:noise parameters applicable to the regional reconstructions.

Extended Data Figure 4. Sensitivity of the onset of sustained significant warming to seasonality. Median onset of sustained, significant warming in regional reconstructions (grey vertical bars; as in Fig. 2a), shown against the grand-median (blue vertical bar), 25–75% range (box) and 5–95% range (horizontal line) of corresponding regional median warming onsets across 10 multi-model Last Millennium climate simulations with full radiative forcings. Dark blue distribution plots (as in Fig. 3a) showing onset of warming where regional temperature information from the models has been extracted for annual or season-specific intervals that match the climate representation of the regional reconstructions (as defined in refs. 4,14). Light blue distributions show for comparison the model results for the median onset of sustained, significant warming using annual average data for the reconstruction regions with a seasonal preference (Europe, Asia, Australasia and South America). The similarity of changepoint results based on annual average or season-specific model data suggests that it is unlikely that seasonality plays a role in the regional characteristics of the onset of sustained, significant warming described in this study.

Extended Data Figure 5. Sensitivity of the onset of sustained significant warming to filter width. Distributions across 15-50y filter widths for the regional onset of sustained, significant warming (Extended Data Fig. 2a) showing the median (grey vertical bar), 25–75% range (grey box) and 5–95% range (grey horizontal line). Coloured/scaled circles demonstrate the changepoints determined at specific filter widths, with markers at 2015CE indicating that a sustained recent warming is not detected. With the exception of Antarctica, where significant warming is not observed at any filter width, the changepoint analysis shows that shorter filter widths (less smoothing) give more recent onset dates for sustained warming. This is because decadal-scale variability resets the time over which significant warming is determined to have been sustained in records with less smoothing. This effect accounts for the wide right-side tails produced in warming onset distributions for the NH reconstruction regions where decadal-scale variability is particularly strong (Fig. 2).

Extended Data Figure 6. Site-level onset of sustained significant trends. a-b, The same SiZer-based trend analysis performed on the regional reconstructions (Methods; Fig. 2a) was applied to individual temperature-sensitive marine and terrestrial records[4,14-16] to determine the median time of onset of sustained and significant industrial-era (a) warming or (b) cooling trends. Where multiple site-level records are available in a 2^{o} x 2^{o} grid region (c; maximum n = 28) the grand-median changepoint is shown in (a) or (b). Symbols are crossed where the interquartile range (i.e. 25–75 percentile range) of changepoints within a grid box exceeds 80 years. In all plots, terrestrial data are shown as square datapoints and marine data are shown as circles. The onset of site-level warming and cooling trends is compiled by latitudinal band in Fig. 4.

Extended Data Figure 7. Moderately resolved marine records and their industrial-era trends. a, Details of the moderate-resolution, SST-sensitive marine records compiled by the Ocean2k working group. For further details on these records we refer readers to ref. 15. b-d, Cumulative distributions of the onset of sustained significant warming (red) or cooling (blue) in subsets of the moderately-resolved marine records. SiZer-based trend analysis was performed on the site-level records and is compiled using the same subsets examined in the "mini-bin" analysis of ref. 15. Shading in (a) denotes records where SiZer analysis detects recent significant cooling trends. The subsets of moderately resolved marine records produce the best differentiation between recent warming and cooling trends when the site-level changepoint results are grouped according to non-upwelling (warming) and upwelling (cooling) sites. This suggests that enhanced ocean upwelling during the Industrial Era may provide a more robust mechanism to account for recent cooling trends in some localised parts of the world oceans, rather than differentiation based on latitude or geochemical analysis type.

Extended Data Figure 8. Onset of sustained significant warming trends in climate simulations. a-d, The same SiZer-based changepoint analysis performed on the regional reconstructions (Methods) was applied to climate simulations compiled at 5^{o}x5^{o} grid resolution to determine the spatial fingerprint for the onset of industrial-era trends. a-b, The multi-model mean for the onset of sustained significant warming in a) surface air temperature and b) sea surface temperature calculated for the first ensemble member of LOVECLIM, CSIRO Mk3L, CCSM4 and HadCM3 Last Millennium experiments with full transient radiative forcings. c-d, as for (a-b) but for the first ensemble member of greenhouse-only forced experiments of the same models. Crosses indicate grid boxes where one or more models produce recent significant cooling rather than warming trends. See Supplementary Figure 3 for results from individual models.

In the subset of models examined here, the fingerprint of warming onset across the oceans is characterised by early warming of most tropical ocean regions except the equatorial eastern Pacific. Delayed warming, or cooling, occurs in the North Atlantic, Arctic and Southern Oceans. The onset of sustained warming is delayed at the grid-level in many terrestrial parts of the NH mid- to high-latitudes due to large decadal-scale model variability over these regions, a feature which is reduced (but still evident; Extended Data Fig. 5) in regionally averaged climate data. The delayed onset of Antarctic warming is not evident in this grid-level assessment, consistent with SH data-model disagreement observed in regionally averaged data.

Extended Data Table 1. High resolution, SST-sensitive coral data compiled by the Ocean2k project. For detailed discussion of the coral database we refer readers to ref. 14. Shading denotes records where SiZer analysis detects recent significant cooling trends (Extended Data Fig. 6b). Strong multi-decadal variability may account for recent SST cooling signals in site-level coral records from Galapagos, Japan and Bermuda, while coral Sr/Ca records from Papua New Guinea are believed to have non-climatic influences.

Extended Data Table 2. Details of the last millennium and historical climate simulations used in this study. The CMIP5 experiment and ensemble member identification for the simulations used in this study. Details are also given for additional idealised forcing experiments examined here. Under CMIP5 protocols[51], Last Millennium simulations cover the period 850–1850CE, and Historical simulations cover the period 1851–2005CE. Note that the number of models that have run the CMIP5 transient last millennium experiment is smaller than the full set of CMIP5 climate models.

Extended Data References

60 Oppo, D. W., Rosenthal, Y. & Linsley, B. K. 2,000-year-long temperature and hydrology reconstructions from the Indo-Pacific warm pool. *Nature* **460**, 1113-1116, doi:10.1038/nature08233 (2009).

61 Pahnke, K., Sachs, J. P., Keigwin, L., Timmermann, A. & Xie, S.-P. Eastern tropical Pacific hydrologic changes during the past 27,000 years from D/H ratios in alkenones. *Paleoceanography* **22**, PA4214, doi:10.1029/2007pa001468 (2007).

62 Hendy, E. J. *et al.* Abrupt decrease in tropical Pacific sea surface salinity at end of Little Ice Age. *Science* **295**, 1511-1514, doi:10.1126/science.1067693 (2002).

63 Hendy, I. L., Dunn, L., Schimmelmann, A. & Pak, D. K. Resolving varve and radiocarbon chronology differences during the last 2000 years in the Santa Barbara Basin sedimentary record, California. *Quaternary International* **310**, 155-168, doi:10.1016/j.quaint.2012.09.006 (2012).

64 Schimmelmann, A., Hendy, I. L., Dunn, L., Pak, D. K. & Lange, C. B. Revised ~2000-year chronostratigraphy of partially varved marine sediment in Santa Barbara Basin, California. *GFF* **135**, 258-264, doi:10.1080/11035897.2013.773066 (2013).

65 Zhao, M., Eglinton, G., Read, G. & Schimmelmann, A. An alkenone ($U_{37}^{K'}$) quasi-annual sea surface temperature record (A.D. 1440 to 1940) using varved sediments from the Santa Barbara Basin. *Organic Geochemistry* **31**, 903-917, doi:10.1016/S0146-6380(00)00034-6 (2000).

66 Gutiérrez, D. *et al.* Coastal cooling and increased productivity in the main upwelling zone off Peru since the mid-twentieth century. *Geophysical Research Letters* **38**, L07603, doi:10.1029/2010gl046324 (2011).

67 Goni, M. A., Thunell, R. C., Woodwort, M. P. & Müller-Karger, F. E. Changes in wind-driven upwelling during the last three centuries: Interocean teleconnections. *Geophysical Research Letters* **33**, L15604, doi:10.1029/2006gl026415 (2006).

68 Doose-Rolinski, H., Rogalla, U. R., Scheeder, G., Lückge, A. & von Rad, U. High-resolution temperature and evaporation changes during the late Holocene in the northeastern Arabian Sea. *Paleoceanography* **16**, 358-367, doi:10.1029/2000pa000511 (2001).

69 Black, D. E. *et al.* An 8-century tropical Atlantic SST record from the Cariaco Basin: Baseline variability, twentieth-century warming, and Atlantic hurricane frequency. *Paleoceanography* **22**, PA4204, doi:10.1029/2007pa001427 (2007).

70 Kuhnert, H. & Mulitza, S. Multidecadal variability and late medieval cooling of near-coastal sea surface temperatures in the eastern tropical North Atlantic. *Paleoceanography* **26**, PA4224, doi:10.1029/2011pa002130 (2011).

71 Leduc, G., Herbert, C. T., Blanz, T., Martinez, P. & Schneider, R. Contrasting evolution of sea surface temperature in the Benguela upwelling system under natural and anthropogenic climate forcings. *Geophysical Research Letters* **37**, L20705, doi:10.1029/2010gl044353 (2010).

72 Richter, T. O., Peeters, F. J. C. & van Weering, T. C. E. Late Holocene (0-2.4 ka BP) surface water temperature and salinity variability, Feni Drift, NE Atlantic Ocean. *Quaternary Science Reviews* **28**, 1941-1955, doi:10.1016/j.quascirev.2009.04.008 (2009).

73 Sicre, M. A. *et al.* Sea surface temperature variability in the subpolar Atlantic over the last two millennia. *Paleoceanography* **26**, PA4218, doi:10.1029/2011pa002169 (2011).

74 Abrantes, F. *et al.* Shallow-marine sediment cores record climate variability and earthquake activity off Lisbon (Portugal) for the last 2000 years. *Quaternary Science Reviews* **24**, 2477-2494 (2005).

75 Versteegh, G. J. M., de Leeuw, J. W., Taricco, C. & Romero, A. Temperature and productivity influences on Uk'_{37} and their possible relation to solar forcing of the Mediterranean winter. *Geochemistry, Geophysics, Geosystems* **8**, Q09005, doi:10.1029/2006gc001543 (2007).

76 Moreno, A. *et al.* The Medieval Climate Anomaly in the Iberian Peninsula reconstructed from marine and lake records. *Quaternary Science Reviews* **43**, 16-32, doi:10.1016/j.quascirev.2012.04.007 (2012).

77 Nieto-Moreno, V. *et al.* Climate conditions in the westernmost Mediterranean over the last two millennia: An integrated biomarker approach. *Organic Geochemistry* **55**, 1-10, doi:10.1016/j.orggeochem.2012.11.001 (2013).
78 Bonnet, S., de Vernal, A., Hillaire-Marcel, C., Radi, T. & Husum, K. Variability of sea-surface temperature and sea-ice cover in the Fram Strait over the last two millennia. *Marine Micropaleontology* **74**, 59-74, doi:10.1016/j.marmicro.2009.12.001 (2010).
79 Felis, T. *et al.* Subtropical coral reveals abrupt early-twentieth-century freshening in the western North Pacific Ocean. *Geology* **37**, 527-530, doi:10.1130/g25581a.1 (2009).
80 Asami, R. *et al.* Interannual and decadal variability of the western Pacific sea surface condition for the years 1787–2000: Reconstruction based on stable isotope record from a Guam coral. *Journal of Geophysical Research: Oceans* **110**, doi:10.1029/2004JC002555 (2005).
81 Charles, C. D., Cobb, K., Moore, M. D. & Fairbanks, R. G. Monsoon–tropical ocean interaction in a network of coral records spanning the 20th century. *Marine Geology* **201**, 207-222 (2003).
82 Boiseau, M., Ghil, M. & Juillet-Leclerc, A. Climatic trends and interdecadal variability from South-Central Pacific coral records. *Geophysical Research Letters* **26**, 2881-2884, doi:10.1029/1999gl900595 (1999).
83 Boiseau, M. *et al.* Atmospheric and oceanic evidences of El Niño-Southern Oscillation events in the south central Pacific Ocean from coral stable isotopic records over the last 137 years. *Paleoceanography* **13**, 671-685, doi:10.1029/98PA02502 (1998).
84 Tudhope, A. W. *et al.* Variability in the El Niño-Southern Oscillation Through a Glacial-Interglacial Cycle. *Science* **291**, 1511-1517, doi:10.1126/science.1057969 (2001).
85 Alibert, C. & Kinsley, L. A 170-year Sr/Ca and Ba/Ca coral record from the western Pacific warm pool: 1. What can we learn from an unusual coral record? *Journal of Geophysical Research-Oceans* **113**, doi:10.1029/2006jc003979 (2008).
86 Quinn, T. M., Taylor, F. W. & Crowley, T. J. Coral-based climate variability in the Western Pacific Warm Pool since 1867. *Journal of Geophysical Research-Oceans* **111**, doi:10.1029/2005jc003243 (2006).
87 Linsley, B. K. *et al.* Tracking the extent of the South Pacific Convergence Zone since the early 1600s. *Geochemistry Geophysics Geosystems* **7**, doi:10.1029/2005gc001115 (2006).
88 Quinn, T. M., Crowley, T. J. & Taylor, F. W. New stable isotope results from a 173-year coral from Espiritu Santo, Vanuatu. *Geophysical Research Letters* **23**, 3413-3416, doi:10.1029/96gl03169 (1996).
89 Gorman, M. K. *et al.* A coral-based reconstruction of sea surface salinity at Sabine Bank, Vanuatu from 1842 to 2007 CE. *Paleoceanography* **27**, doi:10.1029/2012pa002302 (2012).
90 DeLong, K. L., Quinn, T. M., Taylor, F. W., Lin, K. & Shen, C.-C. Sea surface temperature variability in the southwest tropical Pacific since AD 1649. *Nature Climate Change* **2**, 799-804, doi:10.1038/nclimate1583 (2012).
91 DeLong, K. L., Quinn, T. M., Taylor, F. W., Shen, C.-C. & Lin, K. Improving coral-base paleoclimate reconstructions by replicating 350 years of coral Sr/Ca variations. *Palaeogeography Palaeoclimatology Palaeoecology* **373**, 6-24, doi:10.1016/j.palaeo.2012.08.019 (2013).
92 Quinn, T. M. *et al.* A multicentury stable isotope record from a New Caledonia coral: Interannual and decadal sea surface temperature variability in the southwest Pacific since 1657 AD. *Paleoceanography* **13**, 412-426, doi:10.1029/98pa00401 (1998).
93 Bagnato, S., Linsley, B. K., Howe, S. S. & Wellington, G. M. Coral oxygen isotope records of interdecadal climate variations in the South Pacific Convergence Zone region. *Geochemistry Geophysics Geosystems* **6**, doi:10.1029/2004gc000879 (2005).
94 Kuhnert, H., Patzold, J., Wyrwoll, K. H. & Wefer, G. Monitoring climate variability over the past 116 years in coral oxygen isotopes from Ningaloo Reef, Western Australia. *International Journal of Earth Sciences* **88**, 725-732, doi:10.1007/s005310050300 (2000).
95 Druffel, E. R. M. & Griffin, S. Variability of surface ocean radiocarbon and stable isotopes in the southwestern Pacific. *Journal of Geophysical Research-Oceans* **104**, 23607-23613, doi:10.1029/1999jc900212 (1999).

96 Wu, H. C., Linsley, B. K., Dassie, E. P., Schiraldi, B. & deMenocal, P. B. Oceanographic variability in the South Pacific Convergence Zone region over the last 210 years from multi-site coral Sr/Ca records. *Geochemistry Geophysics Geosystems* **14**, 1435-1453, doi:10.1029/2012gc004293 (2013).
97 Linsley, B. K., Ren, L., Dunbar, R. B. & Howe, S. S. El Niño Southern Oscillation (ENSO) and decadal-scale climate variability at 10°N in the eastern Pacific from 1893 to 1994: A coral-based reconstruction from Clipperton Atoll. *Paleoceanography* **15**, 322-335, doi:10.1029/1999PA000428 (2000).
98 Dunbar, R. B., Wellington, G. M., Colgan, M. W. & Glynn, P. W. Eastern Pacific sea-surface temperature since 1600AD: The delta O-18 record of climate variability in Galapagos coral. *Paleoceanography* **9**, 291-315, doi:10.1029/93pa03501 (1994).
99 Urban, F. E., Cole, J. E. & Overpeck, J. T. Influence of mean climate change on climate variability from a 155-year tropical Pacific coral record. *Nature* **407**, 989-993 (2000).
100 Cole, J. E. & Fairbanks, R. G. The Southern Oscillation recorded in the delta O-18 of corals from Tarawa Atoll. *Paleoceanography* **5**, 669-683, doi:10.1029/PA005i005p00669 (1990).
101 Cole, J. E., Fairbanks, R. G. & Shen, G. T. Recent variability in the Southern Oscillation: isotopic results from a Tarawa Atoll coral. *Science* **260**, 1790-1793, doi:10.1126/science.260.5115.1790 (1993).
102 Guilderson, T. P. & Schrag, D. P. Reliability of coral isotope records from the western Pacific warm pool: A comparison using age-optimized records. *Paleoceanography* **14**, 457-464, doi:10.1029/1999pa900024 (1999).
103 Linsley, B. K., Dunbar, R. B., Wellington, G. M. & Mucciarone, D. A. A coral-based reconstruction of intertropical convergence zone variability over central-America since 1707. *Journal of Geophysical Research-Oceans* **99**, 9977-9994, doi:10.1029/94jc00360 (1994).
104 Cobb, K. M., Charles, C. D., Cheng, H. & Edwards, R. L. El Nino/Southern Oscillation and tropical Pacific climate during the last millennium. *Nature* **424**, 271-276, doi:10.1038/nature01779 (2003).
105 Nurhati, I. S., Cobb, K. M., Charles, C. D. & Dunbar, R. B. Late 20th century warming and freshening in the central tropical Pacific. *Geophysical Research Letters* **36**, doi:10.1029/2009gl040270 (2009).
106 Nurhati, I. S., Cobb, K. M. & Di Lorenzo, E. Decadal-Scale SST and Salinity Variations in the Central Tropical Pacific: Signatures of Natural and Anthropogenic Climate Change. *Journal of Climate* **24**, 3294-3308, doi:10.1175/2011jcli3852.1 (2011).
107 Cole, J. E., Dunbar, R. B., McClanahan, T. R. & Muthiga, N. A. Tropical Pacific forcing of decadal SST variability in the western Indian Ocean over the past two centuries. *Science* **287**, 617-619, doi:10.1126/science.287.5453.617 (2000).
108 Zinke, J., Pfeiffer, M., Timm, O., Dullo, W. C. & Brummer, G. J. A. Western Indian Ocean marine and terrestrial records of climate variability: a review and new concepts on land-ocean interactions since AD 1660. *International Journal of Earth Sciences* **98**, 115-133, doi:10.1007/s00531-008-0365-5 (2009).
109 Zinke, J. *et al.* Mayotte coral reveals hydrological changes in the western Indian Ocean between 1881 and 1994. *Geophysical Research Letters* **35**, doi:10.1029/2008gl035634 (2008).
110 Zinke, J., Dullo, W. C., Heiss, G. A. & Eisenhauer, A. ENSO and Indian Ocean subtropical dipole variability is recorded in a coral record off southwest Madagascar for the period 1659 to 1995. *Earth and Planetary Science Letters* **228**, 177-194, doi:10.1016/j.epsl.2004.09.028 (2004).
111 Kuhnert, H. *et al.* A 200-year coral stable oxygen isotope record from a high-latitude reef off western Australia. *Coral Reefs* **18**, 1-12, doi:10.1007/s003380050147 (1999).
112 Damassa, T. D., Cole, J. E., Barnett, H. R., Ault, T. R. & McClanahan, T. R. Enhanced multidecadal climate variability in the seventeenth century from coral isotope records in the western Indian Ocean. *Paleoceanography* **21**, doi:10.1029/2005pa001217 (2006).
113 Abram, N. J., Gagan, M. K., Cole, J. E., Hantoro, W. S. & Mudelsee, M. Recent intensification of tropical climate variability in the Indian Ocean. *Nature Geoscience* **1**, 849-853, doi:10.1038/ngeo357 (2008).
114 Charles, C. D., Hunter, D. E. & Fairbanks, R. G. Interaction between the ENSO and the Asian monsoon in a coral record of tropical climate. *Science* **277**, 925-928, doi:10.1126/science.277.5328.925 (1997).

115 Nakamura, N. *et al.* Mode shift in the Indian Ocean climate under global warming stress. *Geophysical Research Letters* **36**, doi:10.1029/2009gl040590 (2009).
116 Pfeiffer, M., Timm, O., Dullo, W. C. & Podlech, S. Oceanic forcing of interannual and multidecadal climate variability in the southwestern Indian Ocean: Evidence from a 160 year coral isotopic record (La Reunion, 55 degrees E, 21 degrees S). *Paleoceanography* **19**, doi:10.1029/2003pa000964 (2004).
117 Heiss, G. A. Coral reefs in the Red Sea: Growth, production, and stable isotopes., (GEOMAR, Research Center for Marine Geosciences, Christian Albrechts University, 1994).
118 Moustafa, Y. *Paleoclimatic reconstructions of the northern Red Sea during the Holocene inferred from stable isotope records of modern and fossil corals and molluscs* PhD thesis, Berichte aus dem Fachbereich Geowissenschaften der Universitat Bremen, (2000).
119 Felis, T. *et al.* A coral oxygen isotope record from the northern Red Sea documenting NAO, ENSO, and North Pacific teleconnections on Middle East climate variability since the year 1750. *Paleoceanography* **15**, 679-694, doi:10.1029/1999pa000477 (2000).
120 Goodkin, N. F., Hughen, K. A., Curry, W. B., Doney, S. C. & Ostermann, D. R. Sea surface temperature and salinity variability at Bermuda during the end of the Little Ice Age. *Paleoceanography* **23**, doi:10.1029/2007pa001532 (2008).
121 Hetzinger, S., Pfeiffer, M., Dullo, W.-C., Garbe-Schoenberg, D. & Halfar, J. Rapid 20th century warming in the Caribbean and impact of remote forcing on climate in the northern tropical Atlantic as recorded in a Guadeloupe coral. *Palaeogeography Palaeoclimatology Palaeoecology* **296**, 111-124, doi:10.1016/j.palaeo.2010.06.019 (2010).
122 Kilbourne, K. H. *et al.* Paleoclimate proxy perspective on Caribbean climate since the year 1751: Evidence of cooler temperatures and multidecadal variability. *Paleoceanography* **23**, doi:10.1029/2008pa001598 (2008).
123 Kuhnert, H., Cruger, T. & Patzold, J. NAO signature in a Bermuda coral Sr/Ca record. *Geochemistry Geophysics Geosystems* **6**, doi:10.1029/2004gc000786 (2005).
124 Swart, P. K. *et al.* The stable oxygen and carbon isotopic record from a coral growing in Florida Bay: A 160 year record of climatic and anthropogenic influence. *Palaeogeography Palaeoclimatology Palaeoecology* **123**, 219-237, doi:10.1016/0031-0182(95)00078-x (1996).
125 Swart, P. K., Dodge, R. E. & Hudson, H. J. A 240-year stable oxygen and carbon isotopic record in a coral from South Florida: Implications for the prediction of precipitation in Southern Florida. *Palaios* **11**, 362-375, doi:10.2307/3515246 (1996).
126 Saenger, C., Cohen, A. L., Oppo, D. W., Halley, R. B. & Carilli, J. E. Surface-temperature trends and variability in the low-latitude North Atlantic since 1552. *Nature Geoscience* **2**, 492-495, doi:10.1038/ngeo552 (2009).
127 Vasquez-Bedoya, L. F., Cohen, A. L., Oppo, D. W. & Blanchon, P. Corals record persistent multidecadal SST variability in the Atlantic Warm Pool since 1775 AD. *Paleoceanography* **27**, doi:10.1029/2012pa002313 (2012).
128 DeLong, K. L. *et al.* A reconstruction of sea surface temperature variability in the southeastern Gulf of Mexico from 1734 to 2008 CE using cross-dated Sr/Ca records from the coral Siderastrea siderea. *Paleoceanography* **29**, 403-422, doi:10.1002/2013pa002524 (2014).
129 Watanabe, S. *et al.* MIROC-ESM 2010: model description and basic results of CMIP5-20c3m experiments. *Geosci. Model Dev.* **4**, 845-872, doi:10.5194/gmd-4-845-2011 (2011).
130 Bothe, O., Jungclaus, J. H. & Zanchettin, D. Consistency of the multi-model CMIP5/PMIP3-past1000 ensemble. *Clim. Past* **9**, 2471-2487, doi:10.5194/cp-9-2471-2013 (2013).
131 Landrum, L. *et al.* Last Millennium Climate and Its Variability in CCSM4. *J. Clim.* **26**, 1085-1111, doi:10.1175/jcli-d-11-00326.1 (2013).

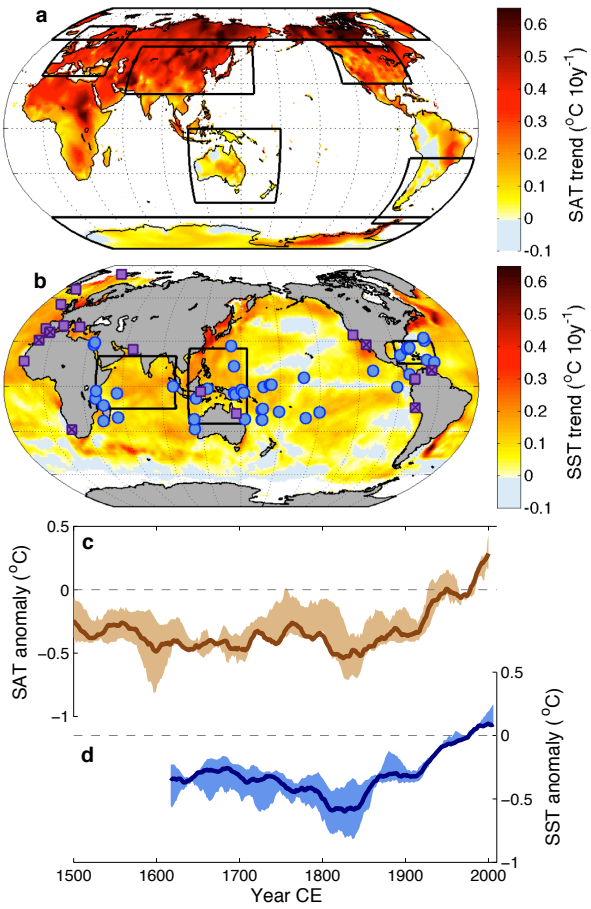
a
0.6
0.5
0.4
0.3
0.2
0.1
0
-0.1
SAT trend (°C 10y-1)
b
0.6
0.5
0.4
0.3
0.2
0.1
0
-0.1
SST trend (°C 10y-1)
c
0.5
0
−0.5
−1
SAT anomaly (°C)
d
0.5
0
−0.5
−1
SST anomaly (°C)
1500
1600
1700
1800
1900
2000
Year CE

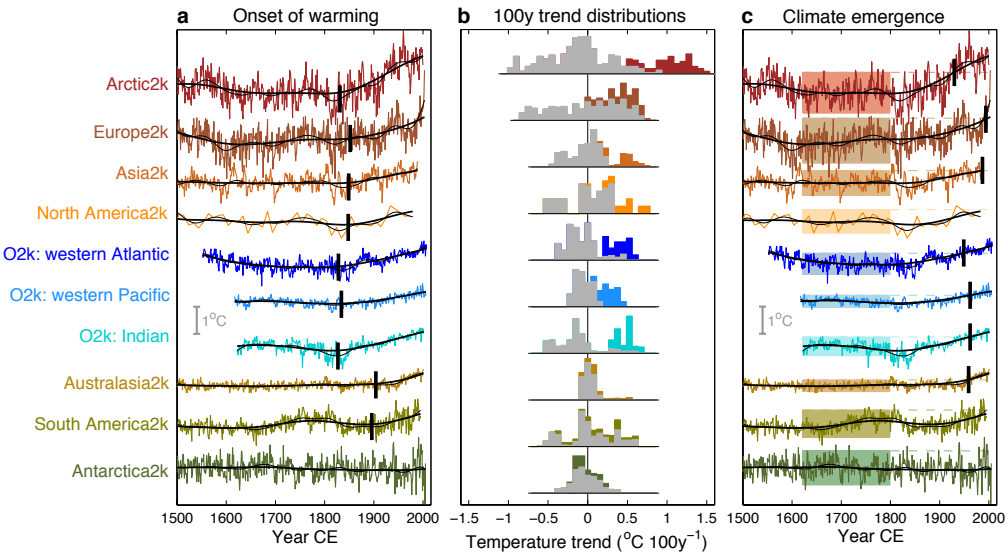
a
Onset of warming
b
100y trend distributions
c
Climate emergence
Arctic2k
Europe2k
Asia2k
North America2k
O2k: western Atlantic
O2k: western Pacific
O2k: Indian
Australasia2k
South America2k
Antarctica2k
1°C
1500 1600 1700 1800 1900 2000
Year CE
−1.5 −1 −0.5 0 0.5 1 1.5
Temperature trend (°C 100y−1)

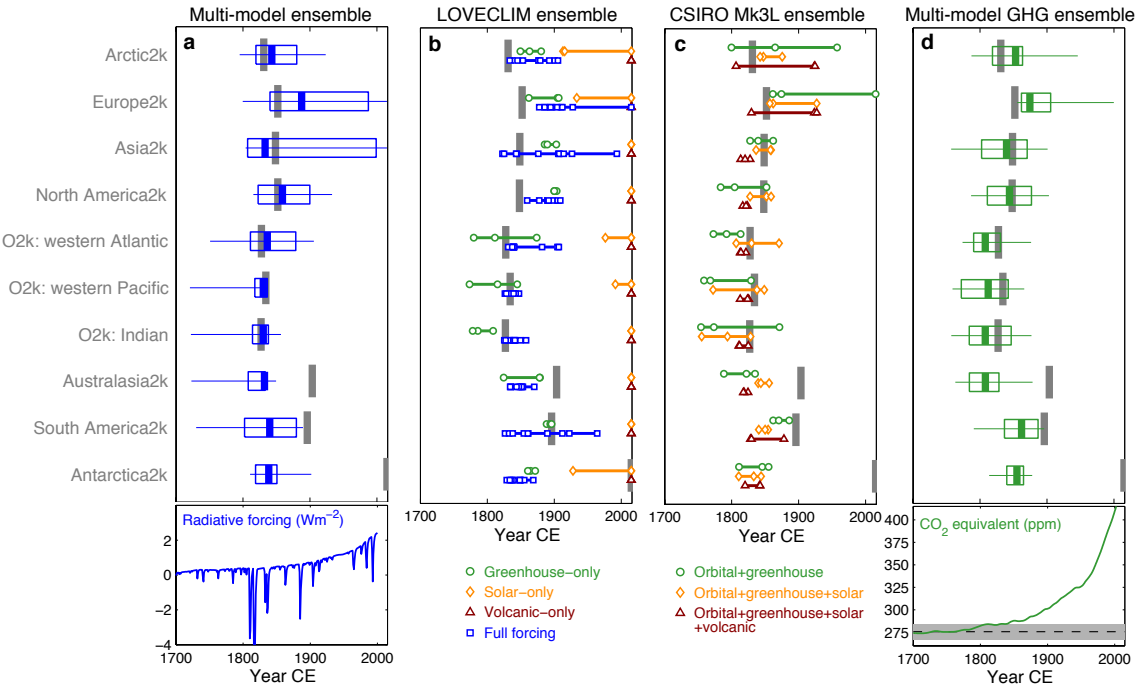
Multi-model ensemble
LOVECLIM ensemble
CSIRO Mk3L ensemble
Multi-model GHG ensemble
a
b
c
d
Arctic2k
Europe2k
Asia2k
North America2k
O2k: western Atlantic
O2k: western Pacific
O2k: Indian
Australasia2k
South America2k
Antarctica2k
Radiative forcing (Wm^{-2})
2
0
−2
−4
1700
1800
1900
2000
Year CE
Greenhouse−only
Solar−only
Volcanic−only
Full forcing
Orbital+greenhouse
Orbital+greenhouse+solar
Orbital+greenhouse+solar +volcanic
CO$_2$ equivalent (ppm)
400
375
350
325
300
275

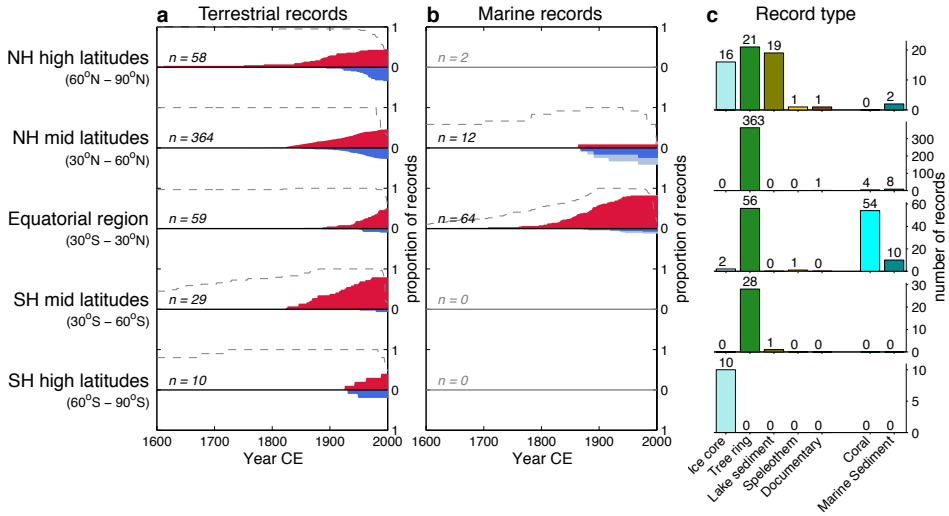
a
Terrestrial records
b
Marine records
c
Record type
NH high latitudes
(60°N – 90°N)
NH mid latitudes
(30°N – 60°N)
Equatorial region
(30°S – 30°N)
SH mid latitudes
(30°S – 60°S)
SH high latitudes
(60°S – 90°S)
n = 58
n = 364
n = 59
n = 29
n = 10
n = 2
n = 12
n = 64
n = 0
n = 0
proportion of records
Year CE
1600
1700
1800
1900
2000
number of records
Ice core
Tree ring
Lake sediment
Speleothem
Documentary
Coral
Marine Sediment

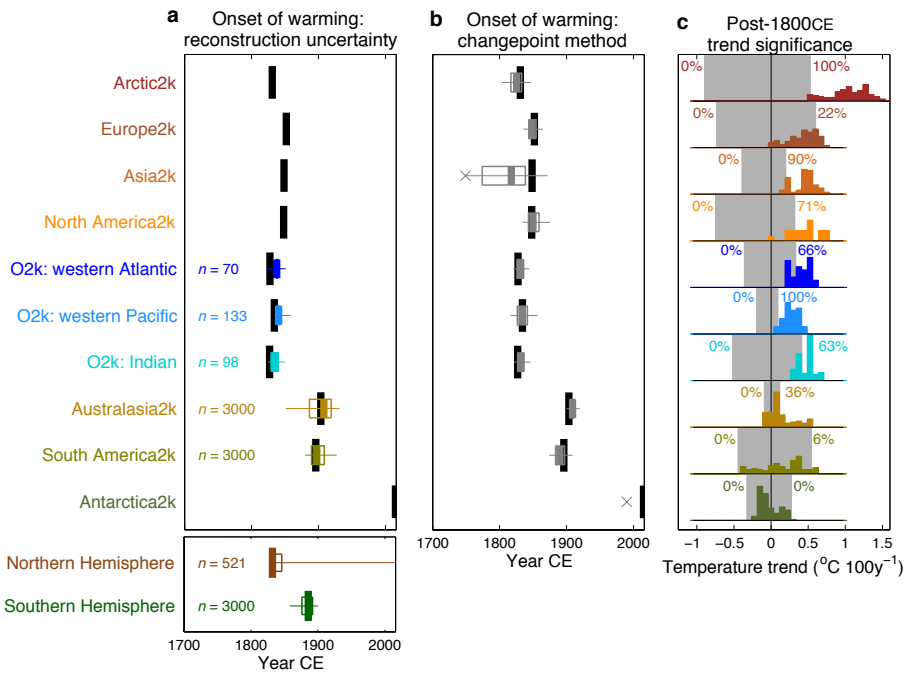
a
Onset of warming:
reconstruction uncertainty
Arctic2k
Europe2k
Asia2k
North America2k
O2k: western Atlantic
n = 70
O2k: western Pacific
n = 133
O2k: Indian
n = 98
Australasia2k
n = 3000
South America2k
n = 3000
Antarctica2k
Northern Hemisphere
n = 521
Southern Hemisphere
n = 3000
1700
1800
1900
2000
Year CE
b
Onset of warming:
changepoint method
1700
1800
1900
2000
Year CE
c
Post-1800CE
trend significance
0%
100%
0%
22%
0%
90%
0%
71%
0%
66%
0%
100%
0%
63%
0%
36%
0%
6%
0%
0%
−1
−0.5
0
0.5
1
1.5
Temperature trend (°C 100y−1)

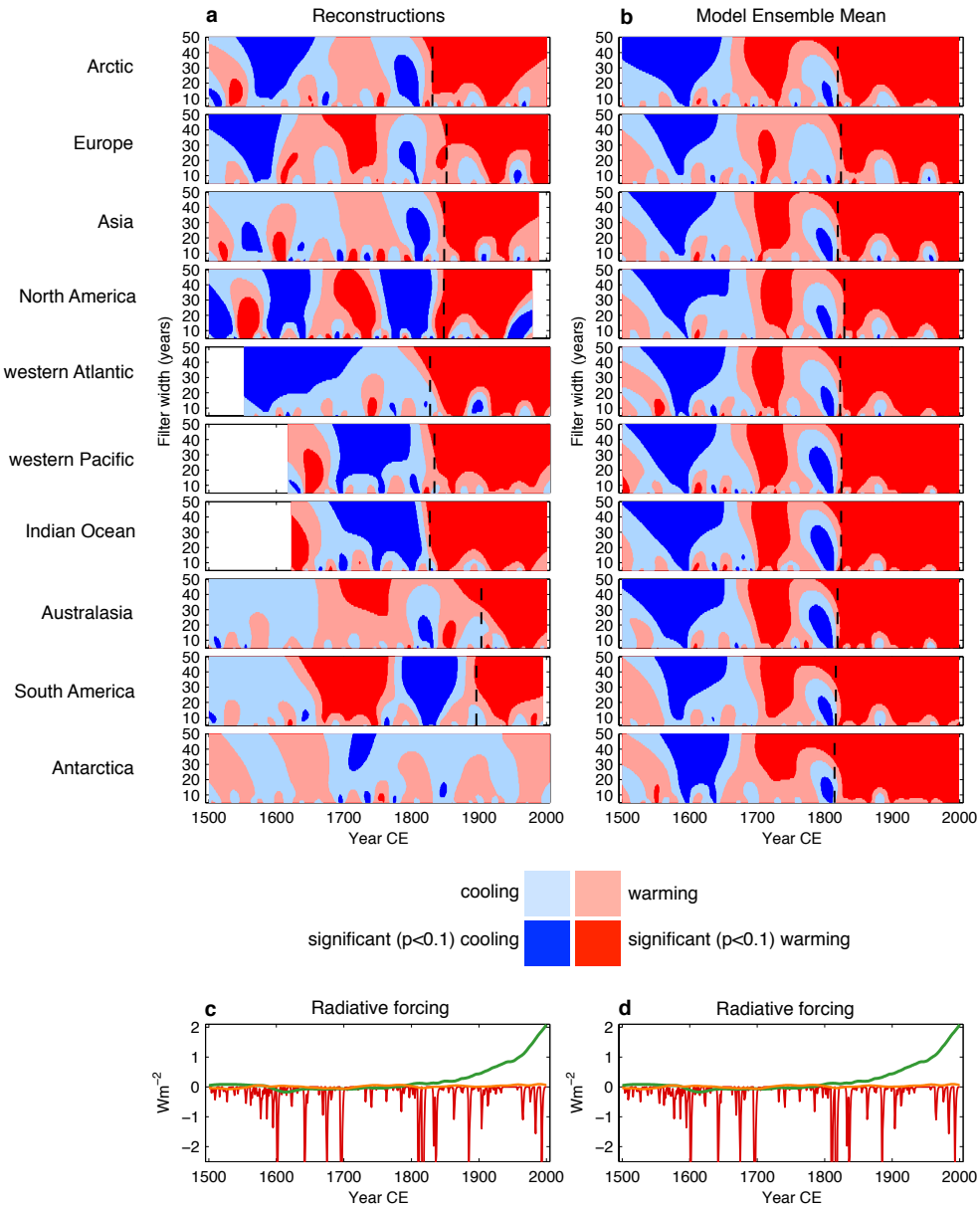
a
Reconstructions
b
Model Ensemble Mean
Arctic
Europe
Asia
North America
western Atlantic
western Pacific
Indian Ocean
Australasia
South America
Antarctica
Filter width (years)
50
40
30
20
10
1500
1600
1700
1800
1900
2000
Year CE
cooling
warming
significant (p<0.1) cooling
significant (p<0.1) warming
c
Radiative forcing
d
Radiative forcing
Wm^{-2}
2
1
0
−1
−2

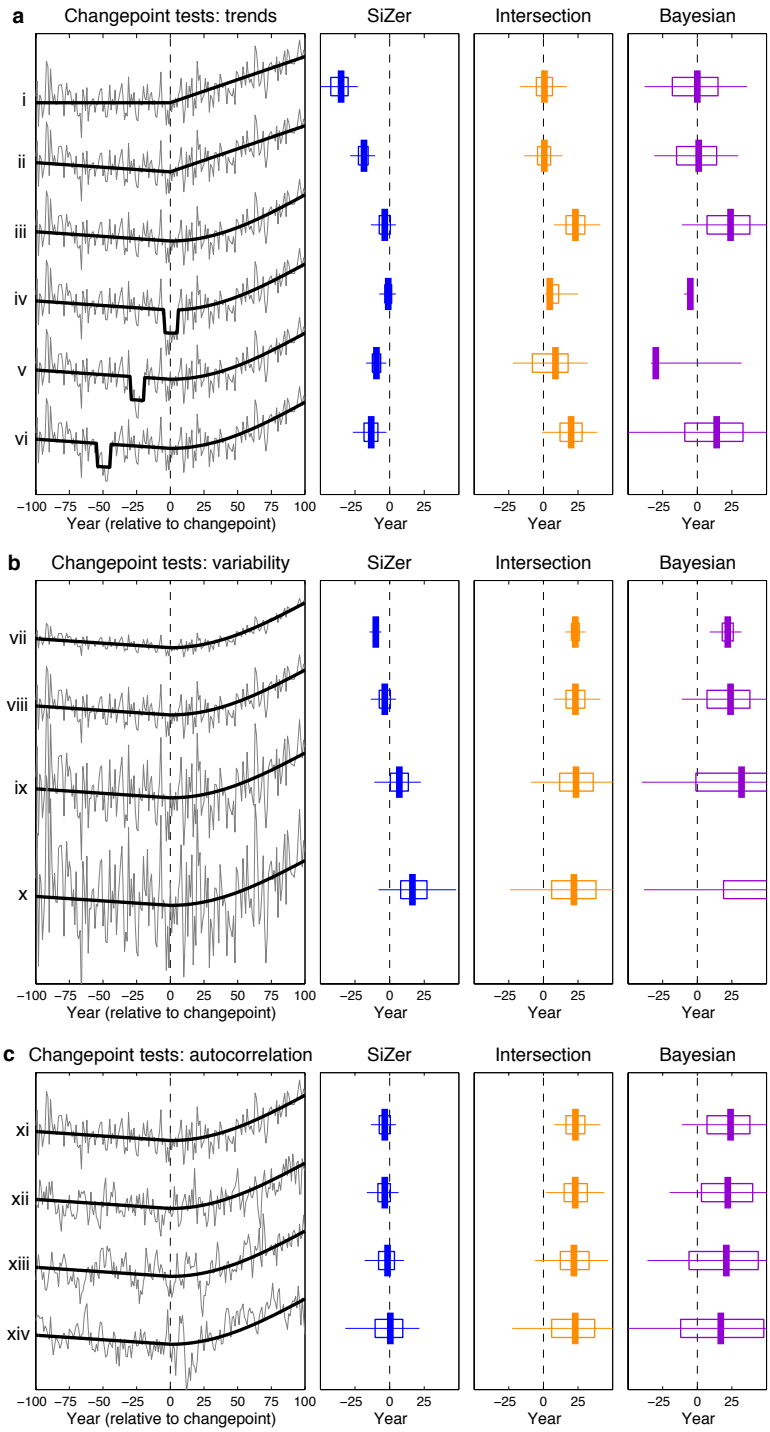
a
Changepoint tests: trends
SiZer
Intersection
Bayesian
i
ii
iii
iv
v
vi
−100 −75 −50 −25 0 25 50 75 100
Year (relative to changepoint)
−25 0 25
Year
b
Changepoint tests: variability
vii
viii
ix
x
c
Changepoint tests: autocorrelation
xi
xii
xiii
xiv

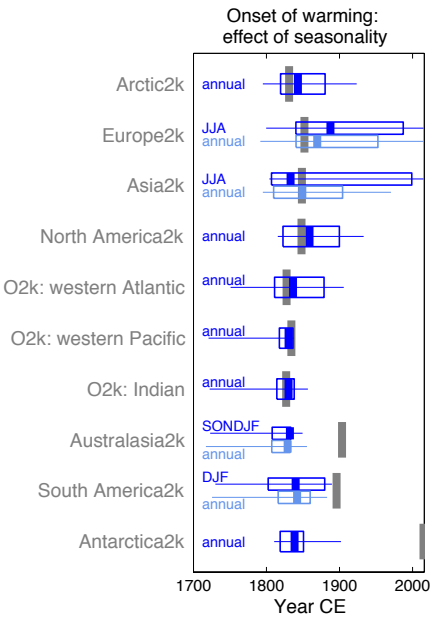
Onset of warming:
effect of seasonality
Arctic2k
annual
Europe2k
JJA
annual
Asia2k
JJA
annual
North America2k
annual
O2k: western Atlantic
annual
O2k: western Pacific
annual
O2k: Indian
annual
Australasia2k
SONDJF
annual
South America2k
DJF
annual
Antarctica2k
annual
1700
1800
1900
2000
Year CE

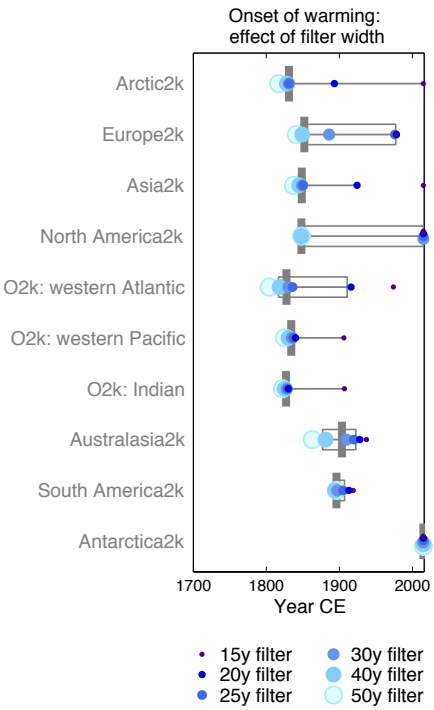
Onset of warming:
effect of filter width
Arctic2k
Europe2k
Asia2k
North America2k
O2k: western Atlantic
O2k: western Pacific
O2k: Indian
Australasia2k
South America2k
Antarctica2k
1700
1800
1900
2000
Year CE
15y filter
20y filter
25y filter
30y filter
40y filter
50y filter

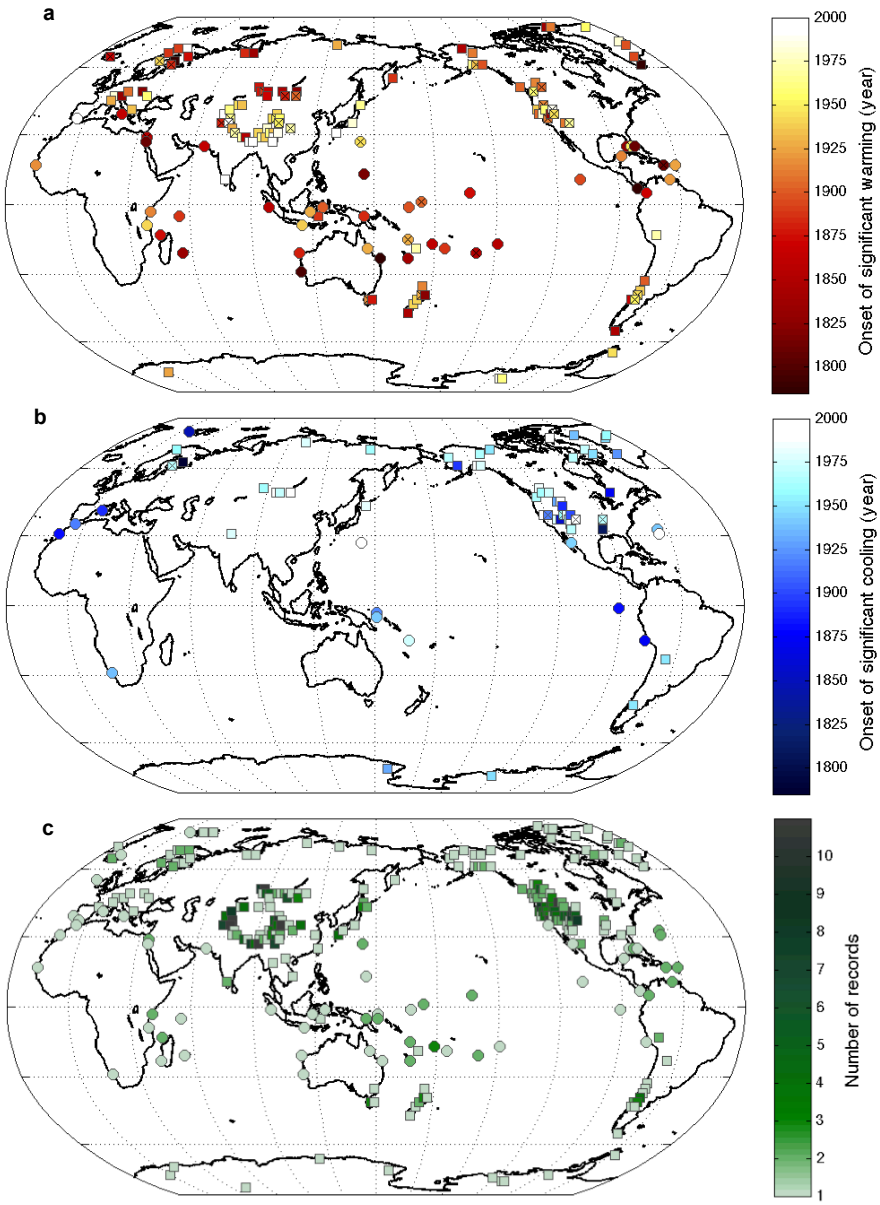
a
2000
1975
1950
1925
1900
1875
1850
1825
1800
Onset of significant warming (year)
b
2000
1975
1950
1925
1900
1875
1850
1825
1800
Onset of significant cooling (year)
c
10
9
8
7
6
5
4
3
2
1
Number of records

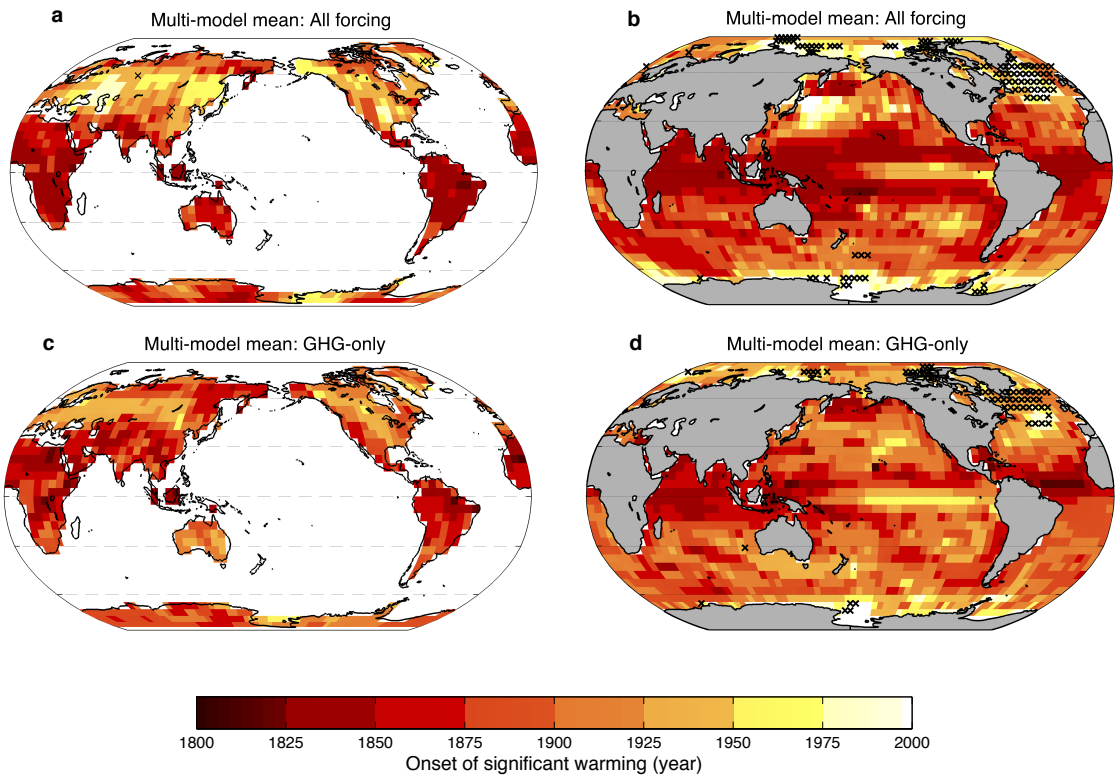
a
Multi-model mean: All forcing
b
Multi-model mean: All forcing
c
Multi-model mean: GHG-only
d
Multi-model mean: GHG-only
1800
1825
1850
1875
1900
1925
1950
1975
2000
Onset of significant warming (year)

a

Ocean basin	Hemi-sphere	Latitude (°N)	Longitude (°E)	Depth (m)	Mean resolution (max/min) (y sample^{-1})	Seasonality	Upwelling /non-upwelling (*a priori*)	Proxy type	Database number[15]	Ref.
Pacific	S	-3.53	119.20	-472	4 (7,<1)	annual	Non	Mg/Ca	0335a	60
Pacific	N	4.67	-77.96	-2200	12(22,11)	annual	Non	alkenone	1177	61
Pacific	N	4.85	-77.61	-884	10(19,9)	annual	Non	alkenone	1178	61
Pacific	S	-18.33	146.45	-10	5(5,5)	annual	Non	coralSr/Ca	1172	62
Pacific	N	34.23	-120.02	-590	1(2,<1)	annual	Non	alkenone	1582	63-65
Pacific	S	-14.13	-76.50	-299	2(5,1)	annual	Upwelling	alkenone	1571	66
Pacific	N	27.90	-111.66	-655	4(9,4)	annual	Upwelling	alkenone	1575	67
Indian	N	24.83	65.92	-695	6(15,<1)	annual	Non	alkenone	1574	68
Atlantic	N	30.85	-10.10	-355	3(6,<1)	annual	Upwelling	alkenone	0487	37
Atlantic	N	10.77	-64.77	-450	1(3,<1)	MAM	Non	Mg/Ca	0039	69
Atlantic	N	16.84	-16.73	-323	3(7,0)	JASOND	Non	Mg/Ca	0488	70
Atlantic	S	-29.14	16.72	-97	4(20,<1)	annual	Upwelling	alkenone	0484	71
Atlantic	N	55.50	-13.90	-84	13(14,11)	AMJJ	Non	Mg/Ca	0058	72
Atlantic	N	66.55	-17.42	-470	3(5,1)	JJA	Non	alkenone	0234	73
Atlantic	N	38.56	-9.35	-90	2(6,<1)	ONDJFMA	Non	alkenone	1183	74
Atlantic	N	10.65	-64.66	-432	5(11,2)	annual	Upwelling	alkenone	1576	67
Med.	N	39.85	17.81	-210	4(4,4)	NDJFM	Non	alkenone	1152	75
Med.	N	40.50	4.03	-2394	16(28,2)	annual	Non	alkenone	1157	76
Med.	N	35.99	-4.75	-1022	6(7,6)	annual	Upwelling	alkenone	1572a	77
Med.	N	36.21	-4.31	-1108	8(12,6)	annual	Upwelling	alkenone	1572b	77
Arctic	N	78.92	6.77	-1497	17(18,16)	annual	Non	dinocyst	1147	78

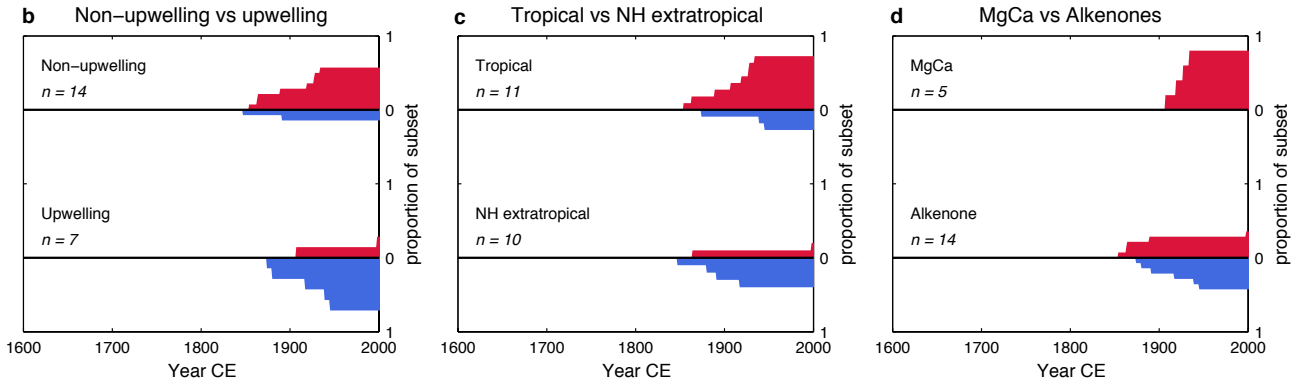

Reconstruction region	Latitude (°N)	Longitude (°E)	Site name	Coral genus	Sampling resolution	Proxy type	References
western Pacific	27.10	142.20	Chichijima	*Porites*	seasonal	Sr/Ca	79
western Pacific	27.10	142.20	Chichijima	*Porites*	seasonal	$\delta^{18}O$	79
western Pacific	13.60	144.83	Double Reef	*Porites*	monthly	$\delta^{18}O$	80
western Pacific	-8.26	115.57	Bali	*Porites*	monthly	$\delta^{18}O$	81
western Pacific	-1.50	124.83	Bunaken	*Porites*	monthly	$\delta^{18}O$	81
western Pacific	-17.50	-149.83	Moorea	*Porites*	annual	$\delta^{18}O$	82,83
western Pacific	-5.22	145.82	Madang	*Porites*	seasonal	$\delta^{18}O$	84
western Pacific	-4.15	144.88	Liang	*Porites*	seasonal	$\delta^{18}O$	84
western Pacific	-2.50	150.5	Kavieng	*Porites*	monthly	Sr/Ca	85
western Pacific	-4.18	151.98	Rabul	*Porites*	monthly	$\delta^{18}O$	86
western Pacific	-4.18	151.98	Rabul	*Porites*	monthly	Sr/Ca	86
western Pacific	-21.24	-159.83	Raratonga*	*Porites*	seasonal	$\delta^{18}O$	87
western Pacific	-21.24	-159.83	Raratonga*	*Porites*	seasonal	Sr/Ca	87
western Pacific	-15.00	166.99	Espiritu Santo	*Porites*	annual	$\delta^{18}O$	88
western Pacific	-15.94	166.04	Sabine Bank*	*Porites*	monthly	$\delta^{18}O$	89
western Pacific	-22.29	166.27	Amedee Island*	*Porites*	monthly	Sr/Ca	90,91
western Pacific	-22.48	166.47	Amadee Island	*Porites*	seasonal	$\delta^{18}O$	92
western Pacific	-16.82	179.23	Suvasuva Bay	*Diploastrea*	annual	$\delta^{18}O$	93
western Pacific	-16.82	179.23	Suvasuva Bay*	*Porites*	annual	$\delta^{18}O$	87
western Pacific	-16.82	179.23	Suvasuva Bay	*Porites*	annual	Sr/Ca	87
western Pacific	-21.91	113.97	Ningaloo Reef	*Porites*	seasonal	$\delta^{18}O$	94
western Pacific	-22.10	153.00	Abraham Reef	*Porites*	annual	$\delta^{18}O$	95
western Pacific	-19.90	-174.70	Tonga	*Porites*	annual	Sr/Ca	96
eastern Pacific	10.28	-109.21	Clipperton Atoll*	*Porites*	seasonal	$\delta^{18}O$	97
eastern Pacific	-0.40	-91.23	Urvina Bay*	*Porites*	annual	$\delta^{18}O$	98
eastern Pacific	1.00	173.00	Maiana Atoll	*Porites*	seasonal	$\delta^{18}O$	99
eastern Pacific	1.00	172.00	Tarawa Atoll	*Porites*	monthly	$\delta^{18}O$	100,101
eastern Pacific	-0.53	166.93	Nauru*	*Porites*	seasonal	$\delta^{18}O$	102
eastern Pacific	7.95	-82.00	Secas Island	*Porites*	seasonal	$\delta^{18}O$	103
eastern Pacific	5.87	-162.13	Palmyra Atoll*	*Porites*	monthly	$\delta^{18}O$	104
eastern Pacific	5.87	-162.13	Palmyra Atoll	*Porites*	monthly	Sr/Ca	105,106
Indian	-3.00	40.00	Malindi	*Porites*	annual	$\delta^{18}O$	107
Indian	-12.65	45.10	Mayotte	*Porites*	seasonal	$\delta^{18}O$	108,109
Indian	-12.65	45.10	Mayotte	*Porites*	seasonal	Sr/Ca	108,109
Indian	-23.15	43.58	Ifaty Reef	*Porites*	seasonal	$\delta^{18}O$	110
Indian	-28.46	113.77	Houtman Abrolhos	*Porites*	seasonal	$\delta^{18}O$	111
Indian	-8.02	39.50	Mafia Island	*Diploastrea*	seasonal	$\delta^{18}O$	112
Indian	-0.13	98.52	Mentawai*	*Porites*	monthly	$\delta^{18}O$	113
Indian	-4.62	55.00	Mahe, Seychelles	*Porites*	monthly	$\delta^{18}O$	114
Indian	-3.20	40.10	Malindi	*Porites*	monthly	$\delta^{18}O$	115
Indian	-21.00	55.00	La Reunion	*Porites*	seasonal	$\delta^{18}O$	116
Indian	29.43	34.97	Aquaba*	*Porites*	annual	$\delta^{18}O$	117
Indian	27.85	34.31	Ras Um Sidd*	*Porites*	seasonal	$\delta^{18}O$	118
Indian	27.85	34.32	Ras Um Sidd	*Porites*	seasonal	$\delta^{18}O$	119
western Atlantic	30.65	-64.99	Bermuda	*Diploria*	annual	$\delta^{18}O$	120
western Atlantic	30.65	-64.99	Bermuda	*Diploria*	annual	Sr/Ca	120
western Atlantic	16.20	-61.49	Guadeloupe	*Diploria*	monthly	$\delta^{18}O$	121
western Atlantic	16.20	-61.49	Guadeloupe	*Diploria*	monthly	Sr/Ca	121
western Atlantic	17.93	-67.00	Puerto Rico	*Montastrea*	annual	$\delta^{18}O$	122
western Atlantic	17.93	-67.00	Puerto Rico	*Montastrea*	annual	Sr/Ca	122
western Atlantic	32.47	-64.70	Bermuda	*Diploria*	monthly	$\delta^{18}O$	123
western Atlantic	32.47	-64.70	Bermuda	*Diploria*	monthly	Sr/Ca	123
western Atlantic	24.93	-80.75	Florida Bay	*Solenastrea*	annual	$\delta^{18}O$	124
western Atlantic	25.38	-80.17	Biscayne, Florida	*Montastrea*	annual	$\delta^{18}O$	125
western Atlantic	25.84	-78.62	Bahamas	*Siderastrea*	annual	growth rate	126
western Atlantic	20.83	-86.74	Yucatan*	*Siderastrea*	annual	growth rate	127
western Atlantic	24.66	-82.83	Dry Tortugas*	*Siderastrea*	monthly	Sr/Ca	128

Model	Sea surface temperature (tos files)		Surface air temperature (tas files)		References
	Last Millennium	Historical	Last Millennium	Historical	
BCC-CSM1.1	past1000_r1i1p1	past1000_r1i1p1	past1000_r1i1p1	past1000_r1i1p1	http://forecast.bcccsm.ncc-cma.net /web/channel-43.htm
MIROC-ESM	past1000_r1i1p1	historical_r1i1p1	past1000_r1i1p1	historical_r1i1p1	129
IPSL CM5A-LR	not available	not available	past1000_r1i1p1	historical_r1i1p1	http://icmc.ipsl.fr/index.php/cmip5
MPI-ESM-P	past1000_r1i1p1	historical_r1i1p1	past1000_r1i1p1	thistorical_r1i1p1	130 http://www.mpimet.mpg.de/en/science/models/mpi-esm.html
NCAR CCSM4	past1000_r1i1p1	historical_r1i1p1	past1000_r1i1p1	historical_r1i1p1	131 http://www.cesm.ucar.edu /experiments/
HadCM3	past1000_r1i1p1	pers. comm	past1000_r1i1p1	pers. comm	20
GISS-E2-R*	past1000_r1i1p124	historical_r1i1p124	past1000_r1i1p124	historical_r1i1p124	http://data.giss.nasa.gov/modelE/ar5/
FGoals-s2	past1000_r1i1p1	pers. comm	not available	not available	
LOVECLIM†	Full forcing (10 member ensemble; e1-e10)		Full forcing (10 member ensemble; e1-e10)		18
LOVECLIM	Greenhouse only (3 member ensemble)		Greenhouse only (3 member ensemble)		18
LOVECLIM	Solar only (3 member ensemble)		Solar only (3 member ensemble)		18
LOVECLIM	Volcanic only (3 member ensemble)		Volcanic only (3 member ensemble)		18
CSIRO-Mk3L v1.2	Orbital + Greenhouse (3 member ensemble)		Orbital + Greenhouse (3 member ensemble)		21
CSIRO-Mk3L v1.2	Orbital + Greenhouse + Solar (3 member ensemble)		Orbital + Greenhouse + Solar (3 member ensemble)		21
CSIRO-Mk3L v1.2†	Orbital + Greenhouse + Solar + Volcanic (3 member ensemble)		Orbital + Greenhouse + Solar + Volcanic (3 member ensemble)		21
HadCM3	Greenhouse only (4 member ensemble)		Greenhouse only (4 member ensemble)		20
NCAR CESM1	Greenhouse only (3 member ensemble)		Greenhouse only (3 member ensemble)		19